26
6-3-80

ornl

OAK
RIDGE
NATIONAL
LABORATORY

UNION
CARBIDE

OPERATED BY
UNION CARBIDE CORPORATION
FOR THE UNITED STATES
DEPARTMENT OF ENERGY

ORNL/TM-7042

MASTER

A Consistent Nuclear Model for Compound and Precompound Reactions with Conservation of Angular Momentum

C. Y. Fu

Printed in the United States of America. Available from
National Technical Information Service
U.S. Department of Commerce
5285 Port Royal Road, Springfield, Virginia 22161
NTIS price codes—Printed Copy: A03; Microfiche A01

ORNL/TM-7042

Contract No. W-7405-eng-26

Engineering Physics Division

A CONSISTENT NUCLEAR MODEL FOR COMPOUND AND PRECOMPOUND REACTIONS WITH CONSERVATION OF ANGULAR MOMENTUM

C. Y. Fu

Date Published - May 1980

OAK RIDGE NATIONAL LABORATORY
Oak Ridge, Tennessee 37830
operated by
UNION CARBIDE CORPORATION
for the
DEPARTMENT OF ENERGY

ABSTRACT

The exciton model of precompound reaction is modified such that it automatically reduces to the usual evaporation formula after equilibrium has been reached. The result is further modified to conserve angular momentum in a form compatible with the Hauser-Feshbach formula. This allows a consistent description of intermediate excitations from which tertiary reaction cross sections can be calculated for transitions to discrete residual levels with known spins and parities. Level densities used for the compound component of reaction cross sections are derived from direct summation of the particle-hole state densities used for the precompound component. Predicted neutron, proton, and alpha-particle production cross sections and spectra from 14-MeV neutron-induced reactions are compared with experimental data. Model parameters of general validity are fixed beforehand. Two parameters are determined from calculations for ^{56}Fe and then used with reasonable success for predicting cross sections for twelve other nuclides.

NUCLEAR REACTIONS ^{27}Al, $^{46,48}Ti$, ^{51}V, $^{50,52}Cr$, $^{54,56}Fe$, $^{58,60}Ni$, $^{63,65}Cu$, ^{93}Nb, E = 14.6 MeV.

Calculated $\sigma(n,xn)$, (n,xp), $(n,x\alpha)$, $\sigma(E_n)$, (E_p), (E_α). Hauser-Feshbach and precompound analysis.

I. INTRODUCTION

Development of fusion energy calls for substantial improvement in the knowledge of neutron cross sections in the energy range from a few MeV to about 40 MeV.[1] In this energy range, the multi-step Hauser-Feshbach model with precompound effects is the most versatile and is considered an indispensible theoretical tool for cross-section evaluations.[2] In analyzing cross sections such as hydrogen and helium production from 14-MeV neutron-induced reactions, we showed[3] that spin and parity effects are more important in the second step of the calculation than in the first step. However, it is not straightforward to conserve angular momentum even in the first step because the presently available models for precompound reactions do not conserve angular momentum. In addition, the compound and precompound components are generally calculated in the first step from two physically different models, thus lacking a common basis for carrying out the calculation to the second step.

In Section III we develop a model capable of calculating the compound and precompound cross sections consistently. The model is further developed in Section IV to conserve angular momentum in both compound and precompound reactions. The model becomes that of Hauser-Feshbach[4] at low energies where precompound effect is negligible. In Section V, level densities used for calculating the compound component are made consistent with those used for the precompound component. Predicted neutron, proton, and alpha-particle production cross sections and spectra from 14-MeV neutron-induced reactions are compared with experimental data in Section VI. The exciton model we started with is summarized first in Section II.

A further motivation behind the present development is our conviction that the conservation of angular momentum is closely related to the capability of calculating angular distributions of outgoing particles, the subject of a second paper in preparation.

II. SUMMARY OF THE EQUILIBRATION PROCESS

The precompound model chosen here as a starting point is the master equation approach[5] rather than the hybrid approach.[6] The latter is simpler but the former provides deeper insight into the equilibration process.

The states of the composite system are enumerated in terms of the number of excited particles, p, and holes, h. For a system with excitation energy E the state density is given by the equations[7]

$$\omega(p,h,E) = \frac{g\ (gE-A_{p,h})^{p+h-1}}{p!\ h!\ (p+h-1)!} \tag{1a}$$

$$A_{p,h} = \frac{p^2+h^2+p-3h}{4} \tag{1b}$$

where g is the density of uniformly-spaced single particle states and the quantity $A_{p,h}$ contains the effects of the Pauli exclusion principle. Particles and holes are often referred to together as excitons with the exciton number of a state given by $n = p + h$.

The residual interactions of the system are assumed to be energy conserving and two-body in nature so that allowed transitions are those for which $\Delta p = \Delta h = 0, \pm 1$. The rates for these transitions are given by the relations[7,8]

$$\lambda_+(p,h,E) = \frac{2\pi}{\hbar} M^2\ \frac{g(gE-C_{p+1,h+1})^2}{2(p+h+1)} \tag{2a}$$

$$\lambda_o(p,h,E) = \frac{2\pi}{\hbar} M^2\ \frac{g}{2}\ (gE-C_{p,h})\ \frac{p^2+h^2+4ph-p-h}{p+h} \tag{2b}$$

$$\lambda_-(p,h,E) = \frac{2\pi}{\hbar} M^2\ \frac{g}{2}\ ph(p+h-2) \tag{2c}$$

$$C_{p,h} = \frac{p^2+h^2}{2} \tag{2d}$$

where M is the average matrix element for an interaction between specific initial and final states, and $C_{p,h}$ contains the effects of the Pauli principle. The quantity M has been evaluated empirically and is given approximately by the relation[9-11]

$$M^2 = k\, A^{-3}\, E^{-1} \ (MeV^3) \tag{3}$$

where k is a scale factor and A is the mass of the composite system.

Particles of type b and energy ε are calculated as being emitted from a state with p particles and h holes at an average rate[5,11]

$$W_b(p,h,\varepsilon)d\varepsilon = \frac{2s_b+1}{\pi^2\hbar^3}\,\mu_b\,\varepsilon\,\sigma_b(\varepsilon)d\varepsilon R_b(p)\,\frac{\omega(p-p_b,h,U)}{\omega(p,h,E)} \tag{4}$$

where, s_b, μ_b, and p_b are the spin, reduced mass and nucleon number of the emitted particle; U is the residual nucleus excitation energy; σ_b is the appropriate inverse reaction cross section; and R_b is a factor which takes account of the distinguishability of protons from neutrons. If p_b nucleons are imagined to be chosen at random from among the p excited particles available, $R_b(p)$ is intended to give the probability that the chosen ones will have the right combination of protons and neutrons to make a particle of type b.

Defining P(p,h,t), the occupation probability, as the probability that the system will be found in a state with p particles and h holes at time t, the master equations which describe the approach of the nucleus to statistical equilibrium are given by[9,11]

$$\frac{dP(p,h,t)}{dt} = P(p-1,h-1,t)\lambda_+(p-1,h-1,E) + P(p+1,h+1,t)\lambda_-(p+1,h+1,E)$$

$$- P(p,h,t)\left[\lambda_+(p,h,E) + \lambda_-(p,h,E) + \sum_b \int_0^{\varepsilon_{max}} W_b(p,h,\varepsilon)d\varepsilon\right] \tag{5}$$

where there is one such equation for each allowed class of particle-hole

configurations. The system is assumed to be formed with unique particle and hole numbers, p_o and h_o so that at time t = 0

$$P(p,h,0) = \delta_{pp_o}\ \delta_{hh_o} \tag{6}$$

which gives the initial conditions for numerical integration of Eq. (5).

Spectra emitted up to the equalibration time T are given by

$$\sigma_b(\varepsilon,T)d\varepsilon = \sigma_{CN} \sum_p W_b(p,h,\varepsilon)d\varepsilon \int_o^T P(p,h,t)dt \tag{7}$$

which gives the precompound component of the energy spectrum of particles of type b. The quantity σ_{CN} is the composite nucleus formation cross section. The equilibration time T is the time when all states in the composite system are equally populated.

III. CONSISTENT COMPOUND AND PRECOMPOUND MODELS

A method is derived for calculating the compound and precompound reaction cross sections consistently. Similar to Eq. (7), spectra emitted from the equilibration time to infinity are given by

$$\sigma_b(\varepsilon,t=T\to\infty)d\varepsilon = \sigma_{CN} \frac{2s_b+1}{\pi^2\hbar^3}\mu_b\ \varepsilon\sigma_b(\varepsilon)d\varepsilon \sum_p R_b(p) \frac{\omega(p-1,h,U)}{\omega(p,h,E)} \int_T^\infty P(p,h,t)dt \tag{8}$$

where p-1 replaces the original factor $p-p_b$ for we shall consider alpha particles as excitons subsequently. The original treatment requires at least four excited nucleons to form an alpha particle. This is virtually impossible for low-energy (14-MeV) nucleon induced reactions. The occupation probability after time T, P(p,h,t>T), as a function of p has the same shape as $\omega(p,h,E)$ for each E. Thus the definition of equilibrium is

$$\frac{P(p,h,t>T)}{\omega(p,h,E)} = C(t,E) \tag{9}$$

where C(t,E) is independent of p or h. It has been shown[7] that for p-1 = h,

$$\sum_p \omega(p-1,h,U) = \frac{\exp(2\sqrt{aU})}{\sqrt{48}\ U} \tag{10}$$

where $a = (\pi^2/6)g$. The right-hand side of Eq. (10) has a form similar to the Fermi gas level density.

It is seen that Eq. (8) would correspond to the compound component if the factor $R_b(p)$ were not there. The problem is due to the fact that the quantities $R_b(p)$ as defined by Kalbach[10] are valid only for t=0, because their values depend entirely on properties of the formation channels. As t approaches T, $R_b(p)$ should approach a constant, otherwise the system cannot be said to be in statistical equilibrium. We now drop the factor $R_b(p)$ and redefine P(p,h,t) as $P_b(p,h,t)$ to serve the same purpose.

The set of master equations reflecting a time-dependent particle-type distribution is given by

$$\frac{d\ P_b(p,h,t)}{dt} = \left[\frac{P_b(p-1,h-1,t)}{P(p-1,h-1,t)}\frac{p-1}{p} + \frac{f_b(p)}{p}\right] P(p-1,h-1,t)\ \lambda_+(p-1,h-1,E)$$

$$+ \left[\frac{P_b(p+1,h+1,t)}{P(p+1,h+1,t)}\right] P(p+1,h+1,t)\ \lambda_-(p+1,h+1,E)$$

$$- P_b(p,h,t)\left[\lambda_+(p,h,E) + \lambda_-(p,h,E) + \int_0^{\varepsilon_{max}} X_b(p,h,\varepsilon)d\varepsilon\right] \tag{11a}$$

with

$$P(p,h,t) = \sum_b P_b(p,h,t) \tag{11b}$$

and

$$\sum_b f_b(p) = 1 \quad . \tag{11c}$$

In Eq. (11), P(p,h,t) is defined similarly to that in Eq. (5) and the ratio $P_b(p,h,t)/P(p,h,t)$ has the same meaning as $R_b(p)$ but is now time-dependent. In the first term in Eq. (11), $P(p-1,h-1,t)\ \lambda_+(p-1,h-1,E)$

represents the total transition rates from (p-1,h-1) states to (p,h) states. Among the p particles in the (p,h) states, (p-1) of them retain the old particle-type distribution $P_b(p-1,h-1,t)/P(p-1,h-1,t)$, but the newly created particle may have a different particle-type distribution given by $f_b(p)$, which will be determined analytically. Thus the compositions of particle types in the new (p,h) states are given by the quantity in the brackets.

In the second term, $P(p+1,h+1,t)\ \lambda_-(p+1,h+1,E)$ represents the total transition rates from (p+1,h+1) states to (p,h) states. The quantity in the brackets is the fraction of particle type b in the (p,h) states. If we assume that various types of particles annihilate with their respective holes at the same rate, then the compositions of various particles in the newly formed (p,h) states are the same as in the initial (p+1,h+1) states.

The emission rates X_b are given by

$$X_b(p,h,\varepsilon)d\varepsilon = \frac{2S_b+1}{\pi^2\hbar^3}\mu_b\ \varepsilon\ \sigma_b(\varepsilon)d\varepsilon\ \frac{\omega_b(p-1,h,U)}{\omega(p,h,E)} \quad . \tag{12}$$

The initial conditions for numerical integration of Eq. (11) are given by

$$P_b(p,h,0) = \delta_{pp_o}\delta_{hh_o}\ q_b \quad , \tag{13}$$

where q_b is the fraction of particle type b in the states (p_o,h_o) at time 0. This fraction is previously contained in $R_b(p_o)$.

We now determine the numerical values of $f_b(p)$ by requiring that $P_b(p,h,T)/\omega(p,h,E)$ be a constant in b and p. The equilibration time T is the time when all allowed states in the composite system are equally populated. If summed over b and the factor $P_b(p,h,t)/P(p,h,t)$ replaced by $R_b(p)$, Eq. (11) reduces to Eq. (5). After equilibrium has been reached, the occupation probabilities P(p,h,t) can be written as

$$P(p,h,t \geq T) = P(t)\ \omega(p,h,E) \quad . \tag{14}$$

In the limit that $\sum_b \int W_b(p,h,\varepsilon)d\varepsilon \ll \lambda_+(p,h,E) + \lambda_-(p,h,E)$, it follows from Eqs. (5) and (14) that

$$\omega(p,h,E)\ \lambda_+(p,h,E) \;=\; \omega(p+1,h+1,E)\ \lambda_-(p+1,h+1,E) \tag{15}$$

which we shall call the condition for the system to stay in equilibrium after time T. Examination of Eqs. (1a), (1b), (2a), and (2c) reveals that Eq. (15) holds only approximately. The reason for this is traced to approximations[8] used in deriving Eq. (2a) for λ_+. We shall renormalize λ_+ such that Eq. (15) holds hereafter. Summing Eq. (11) over b leads to an additional condition which is

$$f_b(p) \;=\; \frac{1}{N} \quad , \tag{16}$$

where N is the number of particle types included in the calculation. Conditions given by the above two equations assure that for $t \geq T$, equilibrium is maintained at all times.

With Eqs. (9), (10), and (11), the particle spectra comprising precompound and compound components, now consistent, are given by

$$\sigma_b(\varepsilon)d\varepsilon \;=\; \sigma_{CN}\,\frac{2S_b+1}{\pi^2\hbar^3}\,\mu_b\,\varepsilon\,\sigma_b(\varepsilon)d\varepsilon\left[\sum_p \frac{\omega_b(p-1,h,U)}{\omega(p,h,E)}\int_0^T P_b(p,h,t)dt + C(E)\,\rho_b(U)\right] \tag{17a}$$

with

$$C(E) \;=\; \int_T^\infty \frac{P_b(p,h,t)dt}{\omega(p,h,E)} \tag{17b}$$

and

$$\rho_b(U) \;=\; \sum_p \omega_b(p-1,h,U) \quad . \tag{17c}$$

The integral in Eq. (17b) can be calculated analytically as follows. Substituting Eqs. (14), (15), and (16) into Eq. (11a) and making use of the identity

$$P(t \geq T) \;=\; N\,P_b(t \geq T) \quad , \tag{18}$$

and summing over b and p, we have

$$\frac{dP(t)}{dt} = -\frac{P(t)}{N}\sum_p \frac{\omega(p,h,E)}{\omega_T}\sum_b \int_0^{\varepsilon_{max}} X_b(p,h,\varepsilon)d\varepsilon \quad , \tag{19}$$

where

$$\omega_T = \sum_p \omega(p,h,E) \quad . \tag{20}$$

Straightforward integration of Eq. (19) yields

$$\int_T^\infty P_b(p,h,t)dt = P(p,h,T) \sum_p \frac{\omega(p,h,E)}{\omega_T}\sum_b \int_o^{\varepsilon_{max}} X_b(p,h,\varepsilon)d\varepsilon, \tag{21}$$

where $P(p,h,T)$ is calculated numerically from Eq. (11). Note that on the right side of Eq. (21) we have $P(p,h,T)$ rather than $P_b(p,h,T)$. This may be understood as follows. After equilibrium has been reached, particle emission may be dominated by one type of particles. Depletion of the occupation probability for this type of particle is then faster than the others, and thus the equilibration process continues. But equilibrium is maintained as long as equilibration is a faster process than particle emission. Therefore, emissions of various types of particles after time T depend only on properties of the residual nuclei — a consequence consistent with the concept of compound nucleus.

The values of $\int_0^T P_b(p,h,t)dt$ for b = n, p, and α, and of $\int_T^\infty P(p,h,t)dt$ as functions of p and h for 14.6-MeV neutrons on ^{63}Cu are shown in Fig. 1. Parameters used for calculations throughout this work are fixed and are presented in Section VI. Figure 1 illustrates the relative strengths of each type of precompound emitted particles and those of compound emitted particles for different p-h states. For example, the ratio of precompound to compound strength is about 16 in exciting 1p-1h states following neutron emission and drops to 0.2 in exciting 2p-2h states.

In conclusion, we emphasize that the compound part of our calculation, as obtained directly from the precompound model developed here, would yield identical results as the conventional compound model as long as $\rho_b(U)$ defined in Eq. (17c) is used in both models. Differences between the p-h state densities and the Fermi-gas level densities in spin distribution and pairing correction are discussed in Section V. A related problem, that of conserving angular momentum in the precompound mode, is addressed first.

IV. CONSERVING ANGULAR MOMENTUM IN THE PRECOMPOUND MODE

In earlier cross-section calculations[3,12] with multi-step Hauser-Feshbach codes containing precompound effects, the precompound components in the first step (binary reaction) were calculated with Eq. (7) or its approximations. The results were then combined with the compound cross sections calculated with the Hauser-Feshbach method.[4] In the second step of calculation (tertiary reaction),[13] the spin populations in the intermediate nuclei are required but are not available from the precompound part of the calculation. Arbitrary assumption has to be made for the spin populations in the intermediate nuclei for the precompound part, violating rules of angular-momentum conservation. We try here to remedy this situation by reducing Eq. (17a) to a form compatible with the Hauser-Feshbach method.

Parallel to the derivation of Eq. (4) by Kalbach[5,11] and taking into account the spin directions in the principle of detailed balance,[14] we decompose the emission rate defined by Eq. (12) into spin-dependent parts:

$$X_b(p,h,J,I,E,\varepsilon)d\varepsilon = \frac{1}{2\pi\hbar} \sum_{s'\ell'} T^J_{bs'\ell'}(\varepsilon)d\varepsilon \frac{\rho_b(p-1,h,I,U)}{\rho(p,h,J,E)} \quad , \qquad (22)$$

where $T^J_{bs'\ell'}$ is the optical-model transmission-coefficient, J is the total spin of the reacting system, I is the spin of the residual level, s' and ℓ' are respectively the channel spin and orbital angular momentum of the emitted particle b. The state density $\omega(p,h,J,E)$ is related to the level density $\rho(p,h,J,E)$ by $\omega(p,h,J,E) = (2J+1)\rho(p,h,J,E)$.

The spin-dependent level densities in Eq. (22) are given by

$$\rho(p,h,J,E) = \omega(p,h,E)\ \rho_n(J) \quad , \qquad (23a)$$

where

$$\rho_n(J) = \frac{1}{2\sqrt{2\pi}\ \sigma_n^3} (2J+1)\ e^{-(J+\frac{1}{2})^2/2\sigma_n^2} \quad , \qquad (23b)$$

with

$$\sigma_n^2 = 1.17\ nc/a \quad , \qquad (23c)$$

where $a = \pi^2 g/6$, and c is a constant related to the moment of inertia.[15] Equation (23c) is derived as follows. At a given excitation energy, the density of levels is dominated by the most probable exciton configurations. The most probable exciton number, $\bar{n}$, corresponding to the particle-hole state densities defined in Eq. (1a) has been derived by Williams[7]

$$\bar{n} = 1.09\ (gE)^{1/2} \quad . \tag{24}$$

The spin-cutoff factor in a Fermi-gas level-density formula, such as given by Gilbert and Cameron,[15] can be equated to $\sigma^2_{\bar{n}}$, leading to

$$\sigma^2_{\bar{n}} = c\tau \quad , \tag{25}$$

where the nuclear temperature, τ, is related to the excitation energy E by

$$E = a\tau^2 \quad . \tag{26}$$

Noting that[16]

$$\sigma^2_n = n\ \sigma^2_1 \quad , \tag{27}$$

Eq. (23c) results. It may be worth noting that σ^2_n is independent of the excitation energy, while $\sigma^2_{\bar{n}}$ increases with $E^{1/2}$.

Our cross-section formula that accounts for both the compound and the precompound effects is a straightforward extension of Eqs. (7) and (8):

$$\sigma_b(E,\varepsilon)d\varepsilon = \pi \lambda^2 \sum_{J\pi} g_J \sum_{s\ell} T^J_{s\ell} \left[\frac{1}{D_{J\pi}} \sum_p X_b(p,h,J,I,E,\varepsilon)\ d\varepsilon \int_0^\infty P_b(p,h,J,t)\ dt \right] \quad , \tag{28a}$$

with

$$D_{J\pi} = \sum_b \sum_{I\pi} \int_\varepsilon \sum_p X_b\ d\varepsilon \int_0^\infty P_b\ dt \quad . \tag{28b}$$

The quantity $D_{J\pi}$ was introduced to ensure that the product inside the brackets of Eq. (28a) has the meaning of a branching ratio. Equation (28) differs from Eq. (17) in exactly the same ways as the Hauser-Feshbach formula is different from the Weisskopf-Ewing evaporation formula, see for example Goldstein.[17]

Computation with Eq. (28) may be drastically simplified if we assume that

$$\frac{P_b(p,h,J,t)}{\omega(p,h,J,E)} = \frac{P_b(p,h,t)}{\omega(p,h,E)} \quad . \tag{29}$$

This assumption enables us to use Eq. (17) directly and amounts to saying that all spin states in the composite system are equally populated during the equilibration process. Noting that the transmission coefficients are independent of the particle-hole indices, we obtain

$$\sigma_b(E,\varepsilon)d\varepsilon = \pi\lambda^2 \sum_{J\pi} g_J \sum_{s\ell} T^J_{s\ell} \frac{d\varepsilon}{D_{J\pi}} \sum_{s'\ell'} T^J_{s'\ell'} \Omega_b(I,E,U) \quad , \tag{30a}$$

where

$$\Omega_b(I,E,U) = \sum_p C_b(p,E)\, \rho_b(p-1,h,I,U) \quad , \tag{30b}$$

with

$$C_b(p,E) = \int_0^\infty P_b(p,h,t)dt/\omega(p,h,E) \quad . \tag{30c}$$

Equation (30) reduces to the usual Hauser-Feshbach formula if instantaneous equilibration is assumed. This amounts to replacing $\int_0^\infty P_b(p,h,t)dt$ by $\omega(p,h,E)$ and $\sum_p \rho_b(p-1,h,I,U)$ by $\rho_b(I,U)$, the conventional level density.

Following the emission of the first particles, the residual levels are populated with certain spin distributions. These spin populations are different for the compound component and the precompound component. As an example, the spin populations in ^{63}Cu following 14.6-MeV (n,n') reaction are shown in Fig. 2 for two outgoing particle energies, 4.5 MeV and 8.5 MeV. Two calculations are compared. The first is based on Eq. (30) which includes precompound effects, and the other is based on the usual Hauser-Feshbach formula. Parameters used for these calculations are presented in Section VI. The precompound effect in spin populations is seen to shift them toward lower spins. The effect is not large at low outgoing particle energies. However, as we have shown previously,[3,13,18] calculations for tertiary reactions such as (n,nα) are quite sensitive to changes in spin populations. In addition, the shift in spin populations is expected to increase with increasing incident particle energies.

Equation (30) may be split up into a compound and a precompound components in the same manner as in Eq. (17). It is convenient to use the Fermi-gas level-density formula for the compound component, particularly at low projectile energies where the precompound effect is negligible. This density formula may differ substantially from that defined in Eq. (17c), partially destroying our attempt at consistency and introducing large uncertainties into our calculations and derived parameters. This problem we now address.

V. LEVEL DENSITIES AND PAIRING CORRECTIONS

For calculations where precompound effect is negligible, it is convenient to use the composite level density formula developed by Gilbert and Cameron.[15] The high energy portion of the formula is

$$\tilde{\rho}_b(U) = \frac{1}{12\sqrt{2}\,\sigma}\,\frac{\exp(2\sqrt{aU'})}{a^{1/4}\,U'^{5/4}} \tag{31}$$

where $\sigma^2 = c\tau$ is used for spin distributions in the usual manner and $U' = U-U_o$. The parameter U_o accounts for the odd-even effect and is often referred to (incorrectly) as the pairing correction. The low energy portion of the composite formula has constant temperature and is normalized to Eq. (31) at E_x, an energy determined empirically.

The formula corresponding to Eq. (31) but based on the p-h level densities is given by

$$\rho_b(U) = \sum_p \frac{1}{\sqrt{2\pi}\,\sigma_n}\,\omega_b(p\text{-}1,h,U) \tag{32}$$

where $\omega_b(p\text{-}1,h,U)$ is given by Eq. (1) and the excitation energy U is used instead of the effective excitation U' in Eq. (31).

The two formulas given by Eq. (31) and Eq. (32) are both based on the uniformly-spaced single particle states. They are, however, very different numerically. The major difference between the two arises from the pairing correction U_o in Eq. (31) and the absence of a comparable correction in Eq. (32). Thus a pairing correction is needed for Eq. (32), at least to account for the odd-even effect.

If an average energy 2Δ is expended to break a nucleon pair, then the minimum energy required to excite p-1 particles and h holes (p-1 = h) are listed below for odd-odd, odd-even, and even-even residual nuclei:

h	odd-odd	odd-even	even-even
1	0	0	2Δ
2	0	2Δ	2Δ
3	2Δ	2Δ	4Δ
4	2Δ	4Δ	4Δ

In odd-odd residual nuclei, for example, at least a pair must be broken in order to excite three particles. Once a pair is broken, a fourth nucleon is already freed, the minimum energy required to excite four particles is also 2Δ.

The maximum energy that may be expended in exciting p-1 particles and h holes is $2h\Delta$, which implies a new pair is always broken in exciting each additional particle. The density of levels that can be formed with this maximum correction is of course small comparing to that with the minimum correction. Therefore, as an approximation, the minimum pairing correction, smoothed over h, may be used for Eq. (32) and is given by

$$U_{p,h} = (h-1.5)\Delta + U_o \quad . \tag{33}$$

The odd-even shift U_o, tabulated by Gilbert and Cameron[15] and adjusted for local effects, is approximately 0 for odd-odd nuclei, Δ for odd-even nuclei, and 2Δ for even-even nuclei. Thus for 1p-1h states, the value of $U_{p,h}$ is approximately -0.5Δ for odd-odd nuclei, 0.5Δ for odd-even nuclei, and 1.5Δ for even-even nuclei. For 2p-2h states, these are 0.5Δ, 1.5Δ, and 2.5Δ respectively. The mass dependence of Δ is given by[20]

$$\Delta = 12/\sqrt{A} \tag{34}$$

The level densities of ^{63}Cu calculated with various formulas discussed above are compared in Fig. 3. Curve 1 represents Eq. (32) with $g = 6a/\pi^2$. Curve 2 is based on the composite formula of Gilbert and Cameron. Curve 3

is based on Eq. (32) but replacing U by $U' = U-U_{p,h}$ with Δ given by Eq. (34). Curve 1 is clearly unacceptable. Curve 3 agrees reasonably with Gilbert and Cameron below 7 MeV. The difference between curve 2 and curve 3 at 7 MeV amounts to 7% change in the parameter a, but becomes larger at higher energies. This may be interpreted as follows.

The pairing correction $U_{p,h}$ increases with increasing hole number. Since the most probable number of excitons at an excitation energy U increases with $U^{1/2}$, the pairing energy correction $U_{p,h}$ increases with $U^{1/2}$ also. For this reason, the correction U_o used in Eq. (31), representing an average of pairing correction for 1p-1h and 2p-2h states, is expected to be too small above 7 MeV, near which the values of U_o are determined. Thus, the level densities calculated from the formula of Gilbert and Cameron is expected to be too high above 7 MeV. In addition, the Pauli-exclusion correction, $A_{p,h}$, in Eq. (32) also reduces curve 3, particularly for high excitation energies. However, its effect is not large comparing to the pairing correction.

We therefore choose to use Eq. (23) for the precompound component and the corresponding quantities summed over p or h for the compound component, both with effective excitation $U' = U-U_{p,h}$, to assure consistency in level densities. More basic and detailed study in the appropriate pairing corrections in both the Fermi-gas and the p-h representations is necessary but is beyond our present purpose.

With the above consideration, Eq. (30) may be split up into the compound and the precompound components by writing Eq. (30b) as:

$$\Omega_b(I,E,U) = \sum_p D_b(p,E)\, \rho_b(p-1,h,I,U') + C(E)\, \rho_b(I,U') \qquad (35a)$$

where

$$D_b(p,E) = \int_0^T P_b(p,h,t)dt/\omega(p,h,E) \qquad (35b)$$

$$C(E) = \int_T^\infty P(p,h,t)dt/\omega(p,h,E) \qquad (35c)$$

$$\rho_b(I,U') = \sum_p \rho_b(p-1,h,I,U') \quad . \qquad (35d)$$

The first term corresponds to precompound and the second compound. This separation is now unnecessary but is computationally convenient.

VI. PARAMETER DETERMINATIONS AND CALCULATIONS

Calculations of neutron, proton, and alpha-particle production spectra for 14.6-MeV neutrons incident on thirteen isotopes are compared with experimental data.[20,21] These calculations are based on Eqs. (30a) and (35). Parameters of general validity are fixed beforehand. Two parameters are determined from calculations for ^{56}Fe and then used for predicting the other twelve isotopes. Calculations shown in Figs. 1 to 3 were based on the same parameters.

Optical model parameters are taken from Wilmore and Hodgson[22] for neutrons, Becchetti and Greenlees[23] for protons, and Huizenga and Igo[24] for alpha-particles. Calculation of gamma-ray transmission coefficients was described previously in detail.[13] Level density parameters are calculated from the empirical formalism of Gilbert and Cameron[15] and used in various formulas throughout this paper. The single particle density g for each nucleus is calculated from the corresponding parameter a and thus has the effect of shell corrections.

A few discrete levels are used for each residual nucleus in the binary step. These levels are given a weight $\Omega_b(I,E,U_c)/\rho_b(I,U_c')$, defined in Eq. (35c) with U_c being the continuum cutoff, such that continuity in the calculated spectra across $E_c \rightarrow U_c$ is maintained. A larger number of discrete levels in each residual nucleus is used in the second step such that more than 80% of decays by proton emission excite the discrete levels. Often only a few discrete levels are excited by the second outgoing particles in (n,np) and (n,nα) reactions. In such cases, the calculated tertiary-reaction cross sections are sensitive to the spacings and spins of the residual discrete levels.

The remaining parameters are k, the scale factor for the residual two-body matrix elements, and q_b, the fraction of particle type b in the states (p_o,h_o) at time 0. A neutron incident on a nucleus sees N neutrons, Z protons, and a maximum of Z/2 alpha clusters. Introducing a parameter f as the clustering probability[11] for alpha particles and using $p_o = 2$ and $h_o = 1$, we have

$$q_n = 0.5\ N/A' + 0.5$$

$$q_p = 0.5\ Z/A'$$

$$q_\alpha = 0.5(0.5\ fZ/A')$$

where $A' = N + Z + 0.5\ fZ$ and the fraction 0.5 accounts for the incident neutron.

The value of k has been determined by Kalbach[11] to be 400 MeV^3. This value depends strongly on the level density parameters. Since the level densities we used here have strong pairing corrections, the value of k is expected to increase. The value k = 700 MeV^3 was determined by fitting the high-energy half of the 14.6-MeV $^{56}Fe(n,xp)$ spectrum measured by Grimes *et al.*[20] as shown in Fig. 4. The (n,xn) spectrum, measured by Hermsdorf *et al.*[21] and integrated over angle by Hetrick *et al.*,[25] was not used for determining the value of k because of possible presence of collective excitations. We have reported[26] DWBA calculations for 15 of the 26 discrete levels up to 4.5 MeV in 14.5-MeV $^{56}Fe(n,n')$ reactions. The dashed histograms in the calculated (n,xn) spectrum in Fig. 4 represent such DWBA calculations. Collective strengths in higher-energy levels may not be negligible, making the determination of the parameter k on (n,xn) spectrum somewhat uncertain.

The (n,xn) spectra measured by Hermsdorf *et al.* are the only set covering all thirteen isotopes studied here. Five other sets of measurements for ^{56}Fe, considered previously,[26] are omitted for clarity. The (n,xp) and (n,xα) spectra measured by Grimes *et al.* are probably the only high quality data available.

After the value of k was determined, the value f = 0.2 was found from the high-energy tail of the $^{56}Fe(n,x\alpha)$ spectrum shown in Fig. 4. This value of f increases the tail of the (n,xα) spectrum near 13 MeV by only 25% from a case calculated with f = 0, thus is weakly determined. A survey[27] of previous calculations for heavier isotopes (A > 100), for which the precompound effect is more pronounced, shows large fluctuations of f with A and shell structures.

With the above parameters, we proceed to predict similar spectra for the other twelve isotopes: ^{27}Al, $^{46,48}Ti$, ^{51}V, $^{50,52}Cr$, ^{54}Fe, $^{58,60}Ni$,

^{63,65}Cu, and ^{93}Nb. The results are compared in Figs. 5 to 17 with experimental data. The (n,xn) data are for natural elements, so are shown separately in Fig. 5. The same data for natural elements are retained in Figs. 6 to 17 for the isotopes, but should be viewed with caution.

The calculated (n,xn) spectra represent sums of partial spectra from (n,n'), 2x(n,2n), (n,pn), and (n,αn) reactions. The (n,xp) spectra are sums of (n,p), (n,pn), and (n,np). The (n,xα) spectra are sums of (n,α), (n,αn), and (n,nα). The dashed curves in Figs. 6 to 17 include calculated results from the first step only. The high-energy edge in each (n,xn) spectrum represents the position of the first excited state in the residual nucleus in (n,n') reaction, while those in the (n,xp) and (n,xα) spectra correspond to the ground states. The dip in the high-energy tail, when present, is from the odd-even shift, which is the most pronounced in even-even residual nucleus.

Best agreement between calculations and experiments is seen for the (n,xp) spectra. This is probably not surprising since the reactions comprising the (n,xp) spectra are rather pure compound and precompound combinations. The measured (n,xn) spectra contain collective excitations. Although DWBA calculations are routinely performed for the low-lying discrete levels for cross-section evaluation works,[14,27,28] it is not straightforward to deal with collective excitations for the continuum states. However, in view of the reasonable agreement between calculated and measured (n,xn) spectra, the collective excitation in continuum states cannot be large in most cases. In several cases, the agreement between calculated and measured (n,xα) spectra is not quite satisfactory. Since the precompound effect is rather small in (n,α) reactions induced by 14.6-MeV neutrons, we speculate that the optical-model parameters used for alpha-particles are not valid for all the isotopes and energies, particularly for low-energy transitions. The conclusion by McFadden and Satchler[29] that a global set of optical-model parameters for alpha-particles could not be found has not yet been challenged.

The pairing corrections impact our calculations in several ways. The odd-even effect scale the level densities in various competing reactions differently, changing the relative magnitudes of cross sections for

these competing reactions. The target nuclei studied here are either even-even or odd Z-even N. For neutron-induced reactions, the composite nuclei are either even Z-odd N or odd-odd. Therefore, the composite nuclei have either non-zero U_o or zero U_o, making the emissions rates defined in Eq. (12) differ as a function of mass for the two types of composite nuclei. Had the odd-even shifts been ignored, two different values of k would have been required for the two types of targets. A third effect concerns the correction $U_{p,h}$, which reduces the slope of all level densities at high energies. A smaller precompound component or a larger k is required. This has the effect of increasing the compound components of all reactions. The cross section of the reaction that has the smallest precompound component is increased most.

The computer code resulted from the present study is dubbed TNG1. This model code is capable of calculating other reaction cross sections not mentioned here, such as capture, (n,3n), (n,2nα), gamma-ray production cross sections and spectra.[3,13] The code has an option to use the level densities of Gilbert and Cameron. In this option, the level densities based on the p-h representation are normalized to the Gilbert and Cameron densities. A smaller value of k (400 MeV^3) is required. With this option, changes in the calculated (n,xn) and (n,xp) spectra are negligible but (n,xα) spectra decreased by up to 30%, resulting in poor overall agreement with experimental data.

Grimes *et al.*[20] calculated (n,xp) and (n,xα) spectra using the multi-step Hauser-Feshbach method for eight of the thirteen isotopes included in the present study. They included the precompound effect for the (n,xp) spectra by a separate model, so their calculations are comparable to what we started out with[3] in this paper. In addition, they did not show their calculated (n,xn) results nor include the precompound effect in the (n,xα) calculations.

By the time this article is ready to be submitted for publication, we have completed some calculations for heavier isotopes, some at shell closures. It became apparent that when large shell correction is incorporated into the single particle level density, g, the parameterization of the residual two-body matrix elements M^2 should be changed from $M^2 = kA^{-3}E^{-1}$ to $M^2 = k'g^{-3}E^{-1}$ to maintain a relatively constant λ_+. Otherwise, the value of k will fluctuate rapidly across shell closures. For example, k was found to be near 10,000 for ^{208}Pb to obtain agreement with experimental (n,xn) data.[21] When $M^2 = k'g^{-3}E^{-1}$ was used, the value k' = 0.3 was found to be quite satisfactory for 18 isotopes from mass 27 to mass 235, including several isotopes near shell closures. An independent conclusion to the same effect has also been obtained by Holub and Cindro.[30] Few other works used shell corrected values for g, a practice that is unrealistic at low incident energies.

VII. CONCLUSIONS

Our consistent treatment of the compound and precompound reactions leads to a single model that reduces to the usual Hauser-Feshbach model at low energies where the precompound effects are negligible. A single set of parameters, including those for level densities, are used for both modes of reactions. For 14.6-MeV neutron-induced reactions, the second outgoing particle often sees only a few discrete levels in the residual nuclei. Therefore, the multi-step Hauser-Feshbach method is used for describing the tertiary reactions. For the same reason, spin populations in the intermediate nuclei are important, and are calculated with conservation of angular momentum in both modes of reaction. Model parameters were determined from one isotope and then used for the prediction of twelve other isotopes. Overall agreement between predicted and measured neutron, proton, and alpha-particle production spectra is reasonably good.

To the best of our knowledge, this is the first time that the three most important competing reactions induced by 14-MeV incident neutrons are calculated simultaneously and compared with experimental data for so many isotopes. The results tend to confirm the neutron and proton occupation probabilities in the initial 2p-1h configurations, a quantity of much diversity in the past.[5,9,31]

Extension of the present model to the calculation of angular distributions is in progress. The extension is based on a partial relaxation of the random phase assumption when precompound reaction is involved. The random phase assumption is that employed in deriving the Hauser-Feshbach model. Therefore, angular distributions are calculated quantum-mechanically and are expected to be forward-peaked in the center-of-mass system when precompound effects are significant. When precompound effects are small, the angular distributions become those of Hauser-Feshbach (front-back symmetry in center-of-mass).

VIII. ACKNOWLEDGEMENTS

The author wishes to thank D. M. Hetrick of Computer Science Division for making most of the calculations and plots, and Prof. C. Kalbach of Duke University for providing the computer code PRECOA, and Dr. R. C. Haight of Lawrence Livermore Laboratory for sending experimental data prior to publication. Critical comments by Drs. R. W. Peelle and J. R. Wu of Oak Ridge National Laboratory are also acknowledged. This work was supported by the United States Department of Energy.

REFERENCES

1. M. R. Bhat and S. Pearlstein, editors, "Symposium on Neutron Cross Sections from 10 to 40 MeV," held at Brookhaven National Laboratory, Upton, New York 11973, May 3-5, 1977, BNL-NCS-50681 (1977).
2. L.Stewart and E. D. Arthur, "Neutron Cross-Section Evaluation at High Energies - Problems and Prospects," p. 435, reference 1.
3. C. Y. Fu, "Multi-Step Hauser-Feshbach Codes with Precompound Effects: A Brief Review of Current and Required Developments and Applications up to 40 MeV," p. 453, reference 1.
4. W. Hauser and H. Feshbach, Phys. Rev. 87, 366 (1952).
5. C. K. Cline and M. Blann, Nucl. Phys. A172, 225 (1971).
6. M. Blann, Nucl. Phys. A213, 570 (1973).
7. F. C. Williams, Jr., Nucl. Phys. A166, 231 (1971).
8. I. Ribansky, P. Oblozinsky, and E. Betak, Nucl. Phys. A205, 545 (1973).
9. C. K. Cline, Nucl. Phys. A195, 353 (1972).
10. C. Kalbach-Cline, Nucl. Phys. A210, 590 (1973).
11. C. Kalbach, Z. Physik A283, 401 (1977).
12. E. D. Arthur and P. G. Young, "Cross Sections in the Energy Range from 10 to 40 MeV Calculated with the GNASH Code," p. 467, reference 1.
13. C. Y. Fu, Atomic Data and Nucl. Data Tables 17, 127 (1976).
14. L. R. B. Elton, Introductory Nuclear Theory (Interscience Publishers, Inc., New York, 1959) p. 137.
15. A. Gilbert and A. G. W. Cameron, Can. J. Phys. 43, 1446 (1965).
16. H. A. Bethe, Phys. Rev. 50, 332 (1936).
17. H. Goldstein, in Fast Neutron Physics, edited by J. B. Marion and J. L. Fowler, Vol. 2 (Interscience Publishers, Inc., New York, 1963) p. 1525.
18. C. Y. Fu and F. G. Perey, J. Nucl. Mat. 61, 153 (1976).
19. A. Bohr and B. R. Mottelson, Nuclear Structure (W. A. Benjamin, Inc., New York, 1969) p. 169.
20. S. M. Grimes, R. C. Haight, K. R. Alvar, H. H. Barschall, and R. R. Borchers, Phys. Rev. C19, 2127 (1979). R. C. Haight and S. M. Grimes, Lawrence Livermore Laboratory Report UCRL-80235 (1977) and private communication.
21. D. Hermsdorf, A. Meister, S. Sassonoff, D. Seeliger, K. Seidel, and F. Shahin, Zentralinstitut für Kernforschung, Rossendorf Bei Dresden, ZfK-277 (Ü), (1975).
22. D. Wilmore and P. Hodgson, Nucl. Phys. 55, 673 (1964).
23. F. D. Becchetti and G. W. Greenlees, Phys. Rev. 182, 1190 (1969).

24. J. R. Huizenga and G. J. Igo, Nucl. Phys. 29, 462 (1962).

25. D. M. Hetrick, D. C. Larson, and C. Y. Fu, Oak Ridge National Laboratory Report ORNL/TM-6637, ENDF-280 (1979).

26. C. Y. Fu, in Nuclear Cross Sections and Technology, Proceedings of a Conference, Vol. I, p. 328, National Bureau of Standards Special Publication SP-425, Washington, D. C., 1975.

27. H. J. Mang, in Proceedings of the Second International Conference on Clustering Phenomena in Nuclei, Vol. II, p. 601, College Park, Maryland, 1975.

28. C. Y. Fu and F. G. Perey, Atomic Data and Nucl. Data Tables 16, 409 (1975).

29. L. McFadden and G. R. Satchler, Nucl. Phys. 84, 177 (1966).

30. E. Holub, Institute Rudjer Boskovic, Zagreb, Yugoslavia, private communication (1980).

31. S. K. Gupta, Bhabha Atomic Research Center, Bombay, India, private communication (1980).

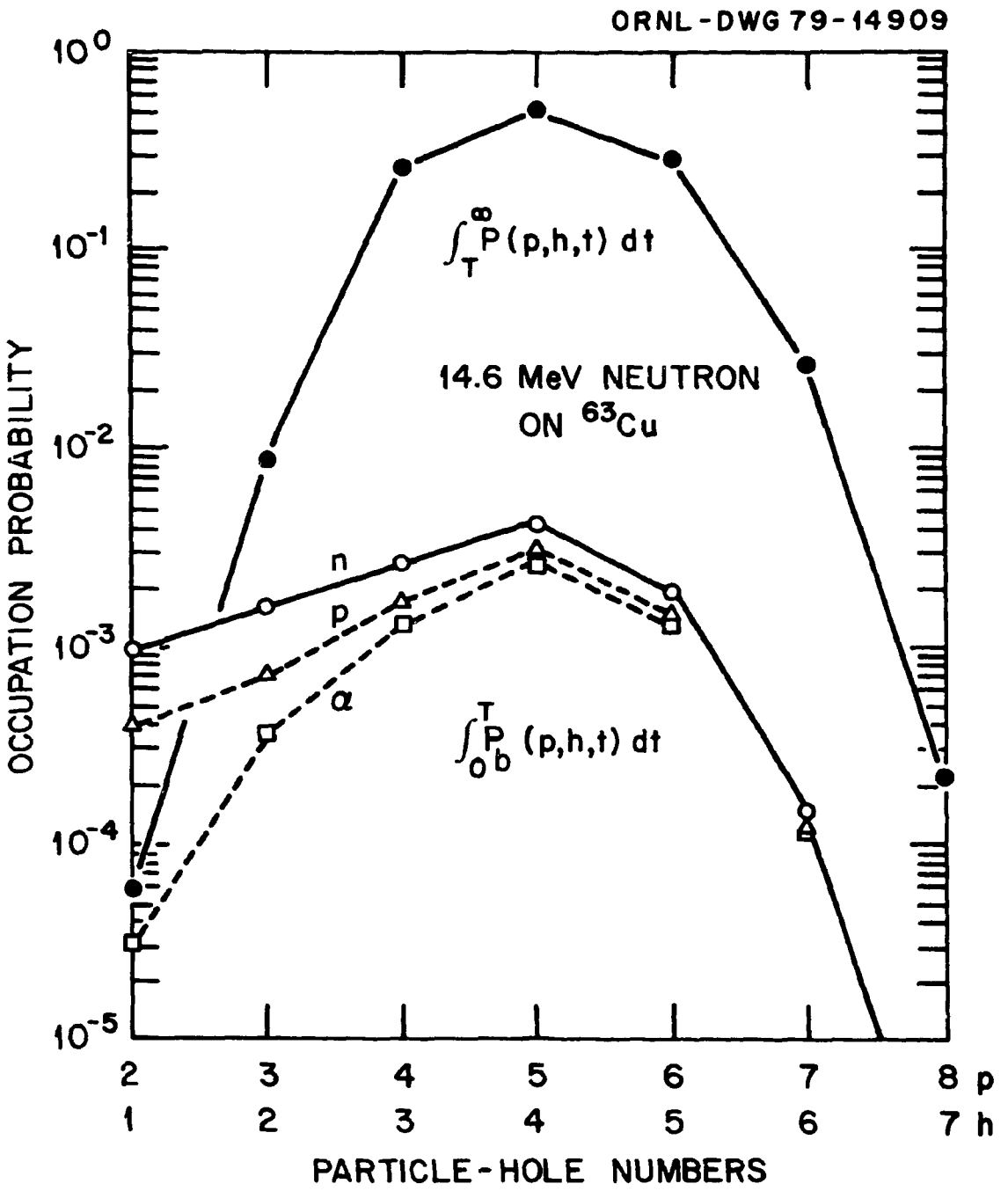

Fig. 1. Time-integrated occupation probabilities for 14.6-MeV neutrons on ^{63}Cu.

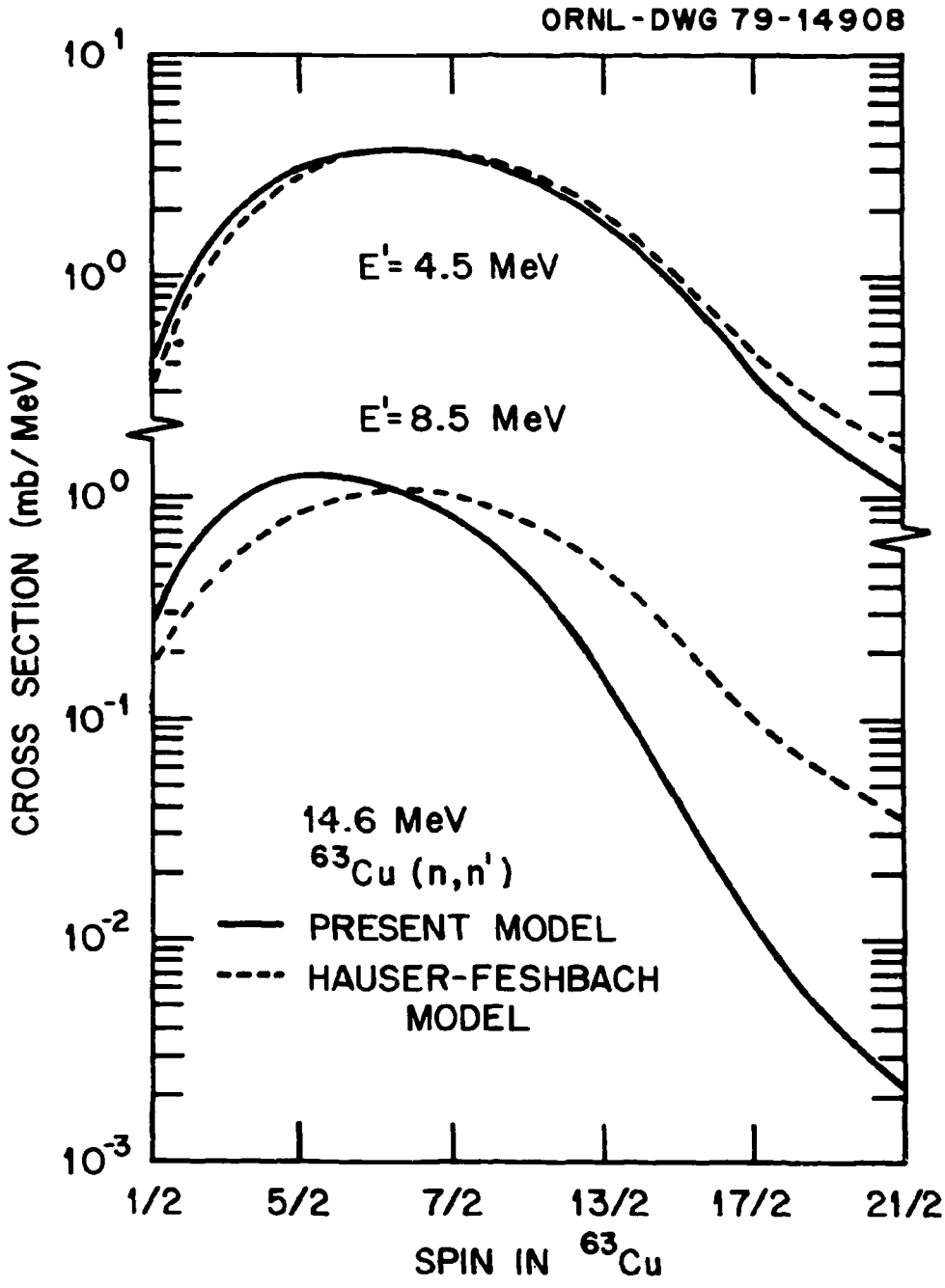

Fig. 2. Spin populations in ^{63}Cu following 14.6-MeV (n,n') reaction for two outgoing neutron energies, E' = 4.5 MeV and E' = 8.5 MeV. The solid curves are based on the present model which includes precompound effects. The dashed curves are based on the Hauser-Feshbach method.

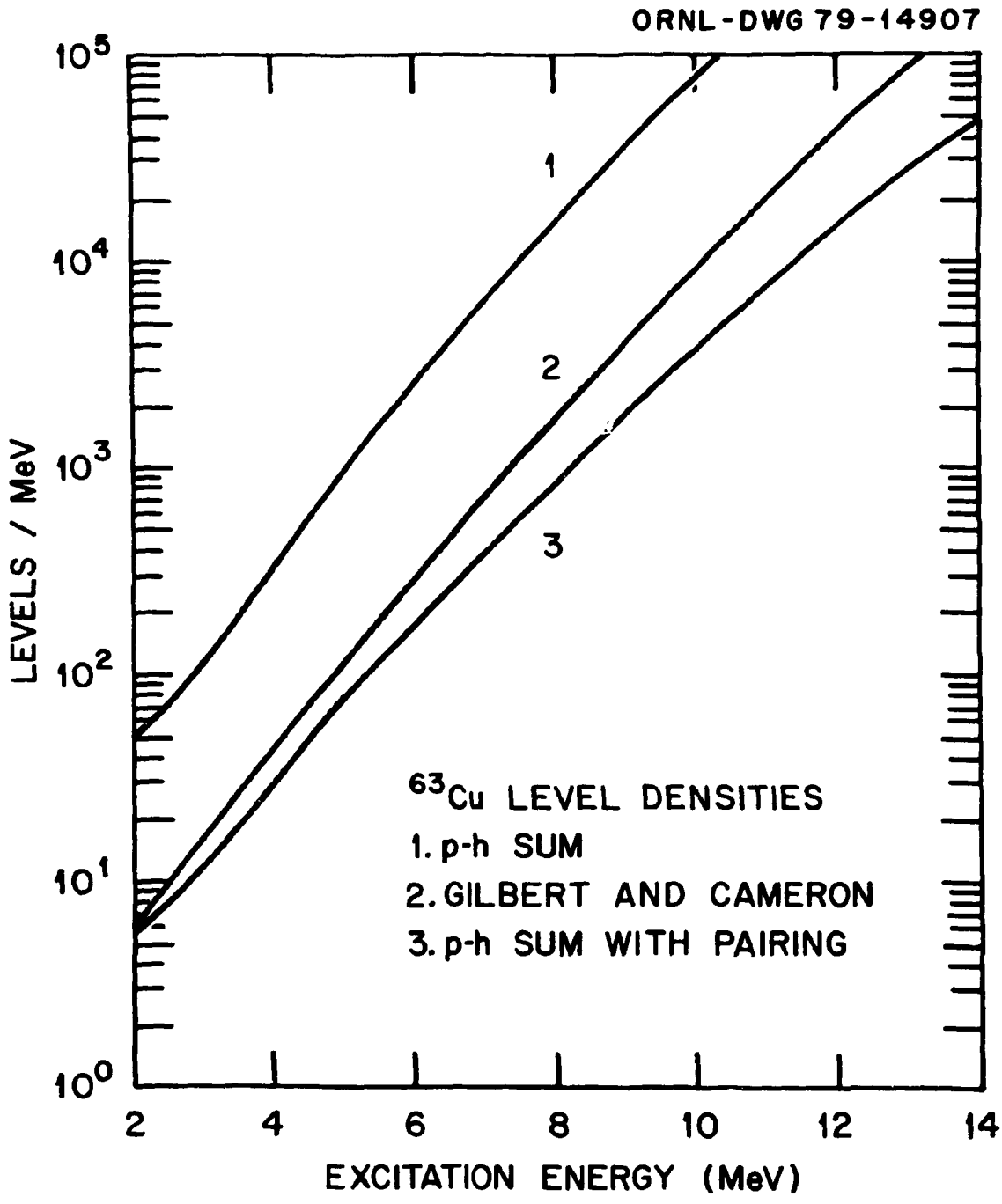

Fig. 3. ^{63}Cu level densities calculated with various formulas.

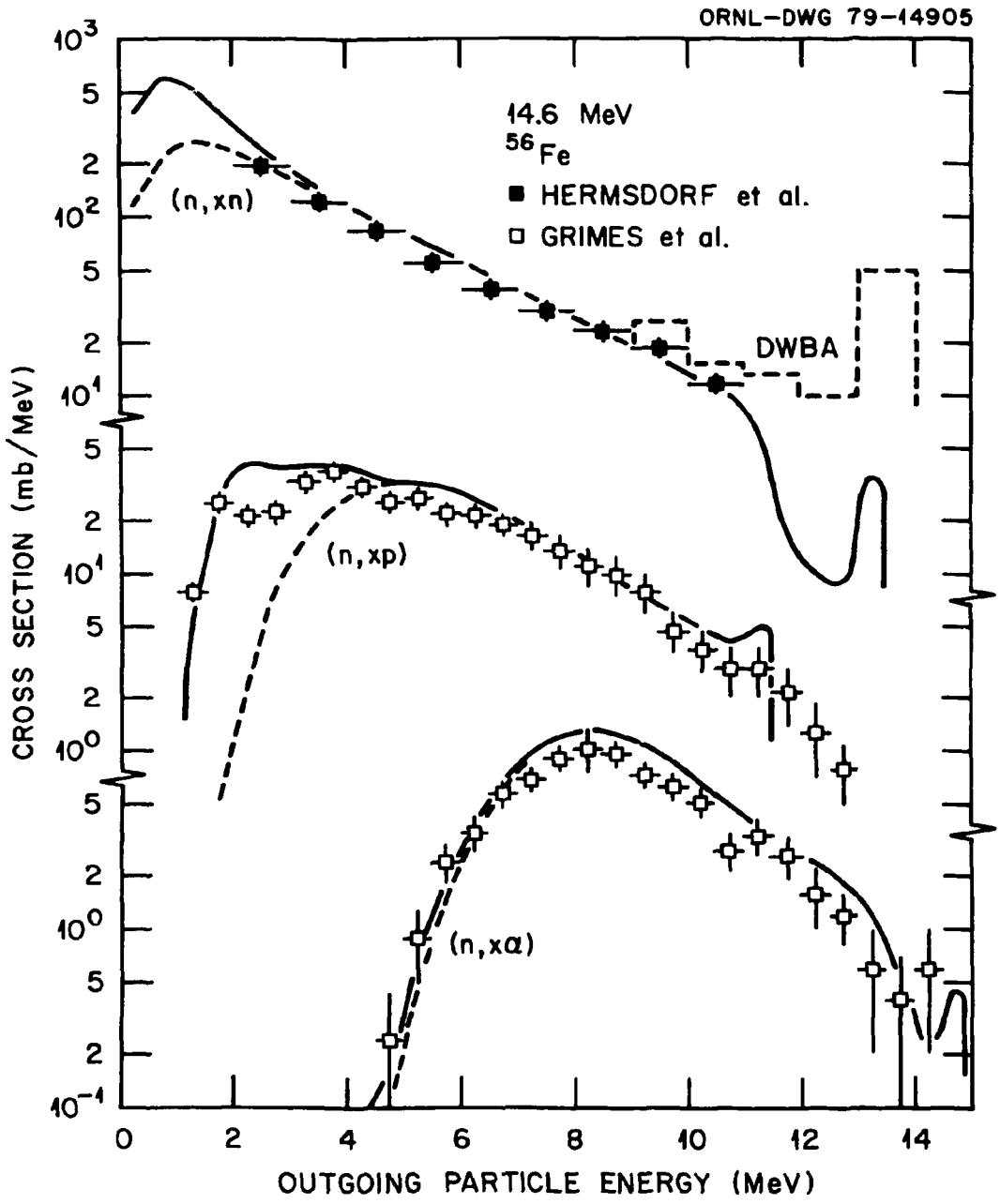

Fig. 4. Calculated and experimental n, p, α production spectra from 14.6-MeV neutrons on ^{56}Fe. The solid curves are calculations. The dashed curves include calculated contributions from the binary step only. The histograms represent DWBA calculations of (n,n') cross sections for 15 discrete levels.

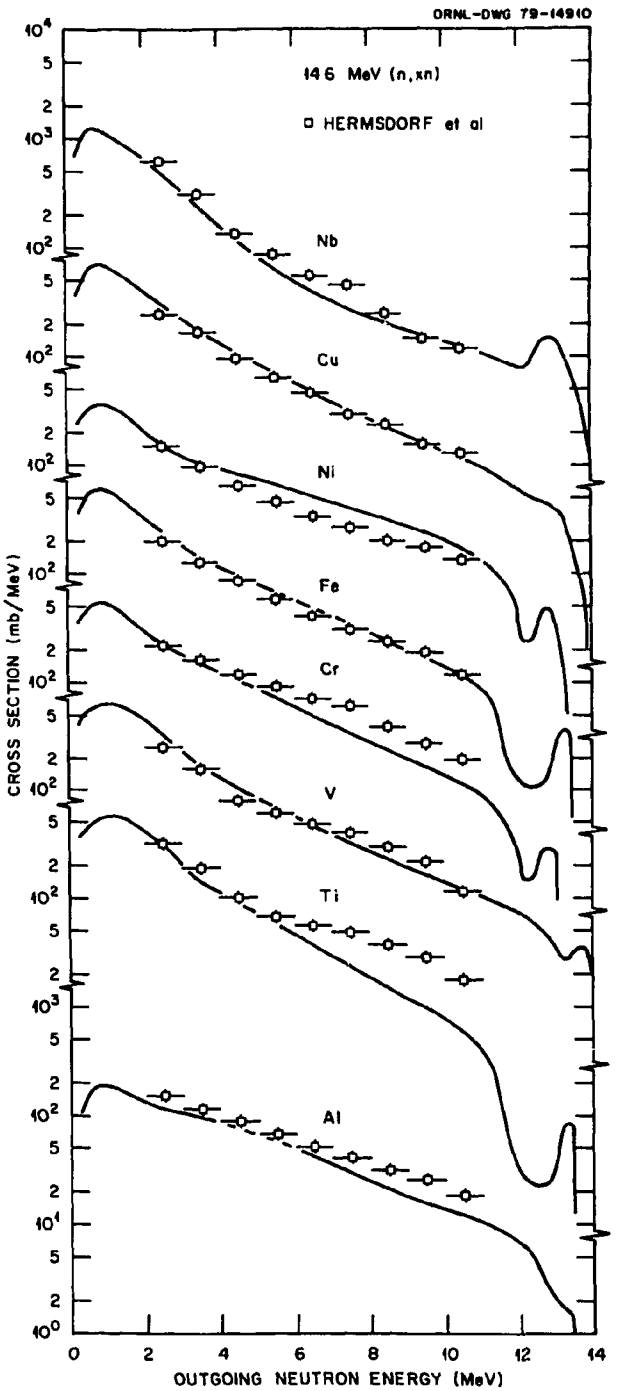

Fig. 5. Calculated and experimental neutron production spectra from 14.6-MeV neutrons on eight natural elements. See Figs. 6-17 for results calculated for individual isotopes.

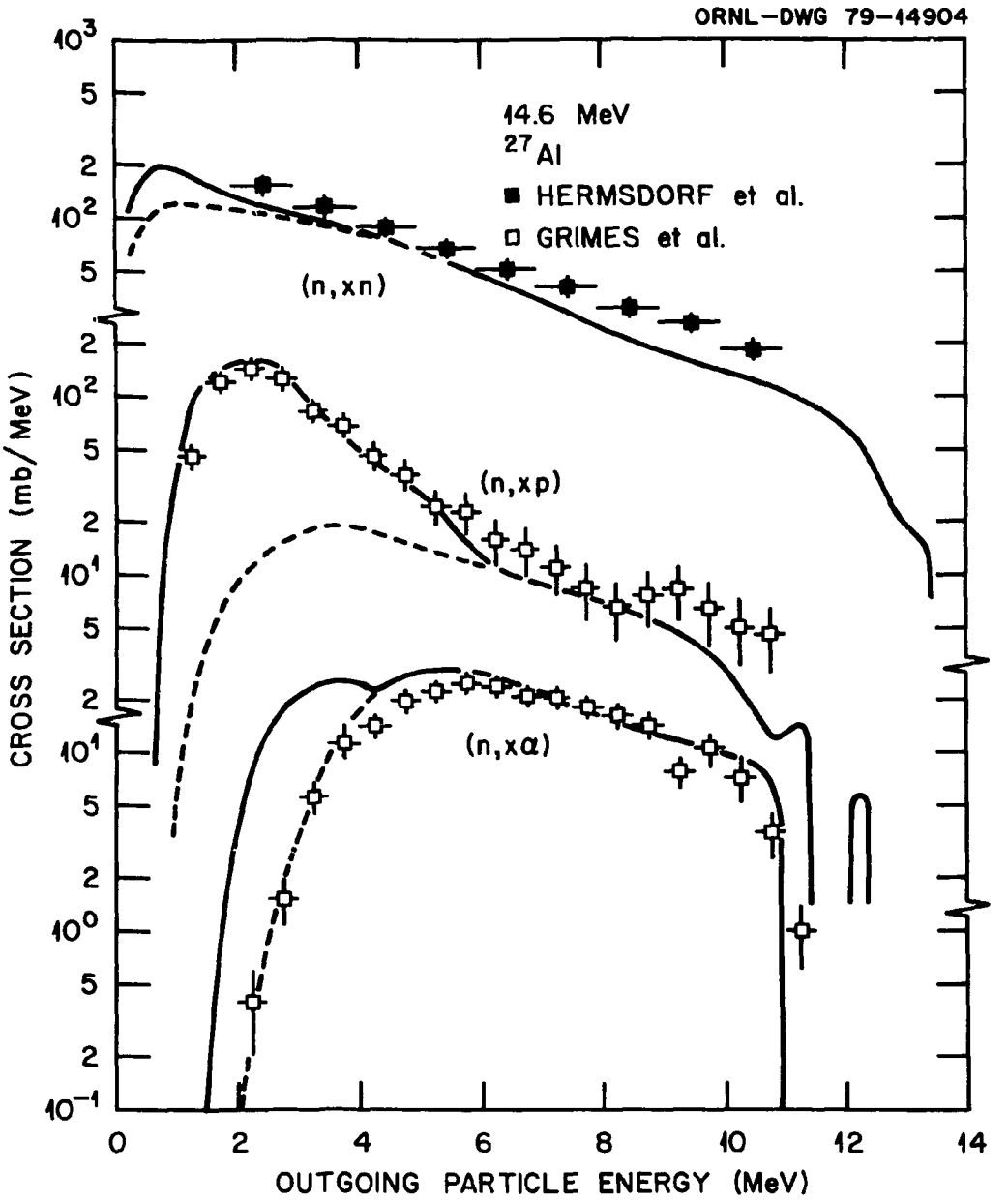

Fig. 6. Calculated and experimental n, p, α production spectra from 14.6-MeV neutrons on ^{27}Al. The dashed curves include contributions from the binary step only.

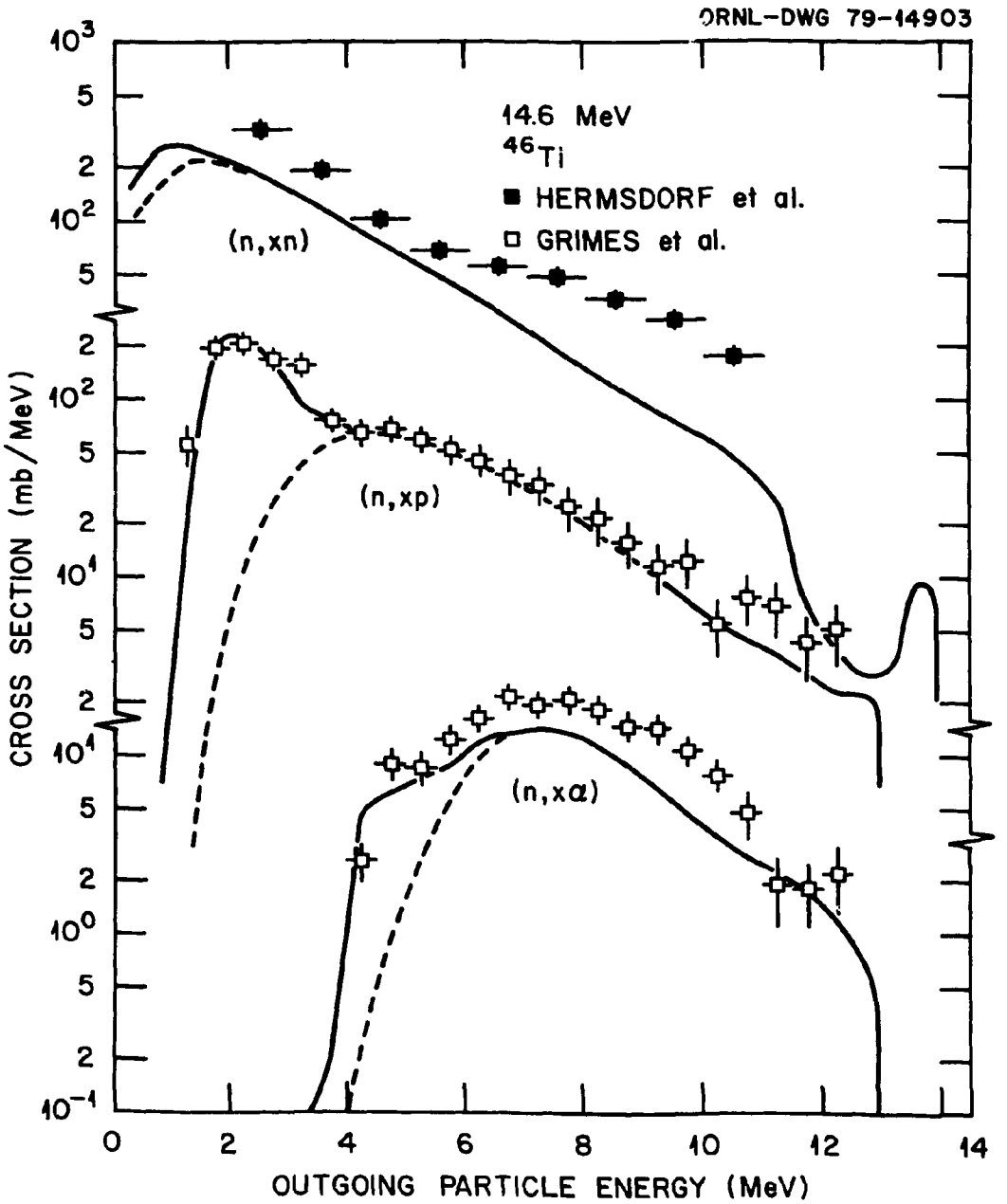

Fig. 7. Calculated and experimental n, p, α production spectra from 14.6-MeV neutrons on ^{46}Ti.

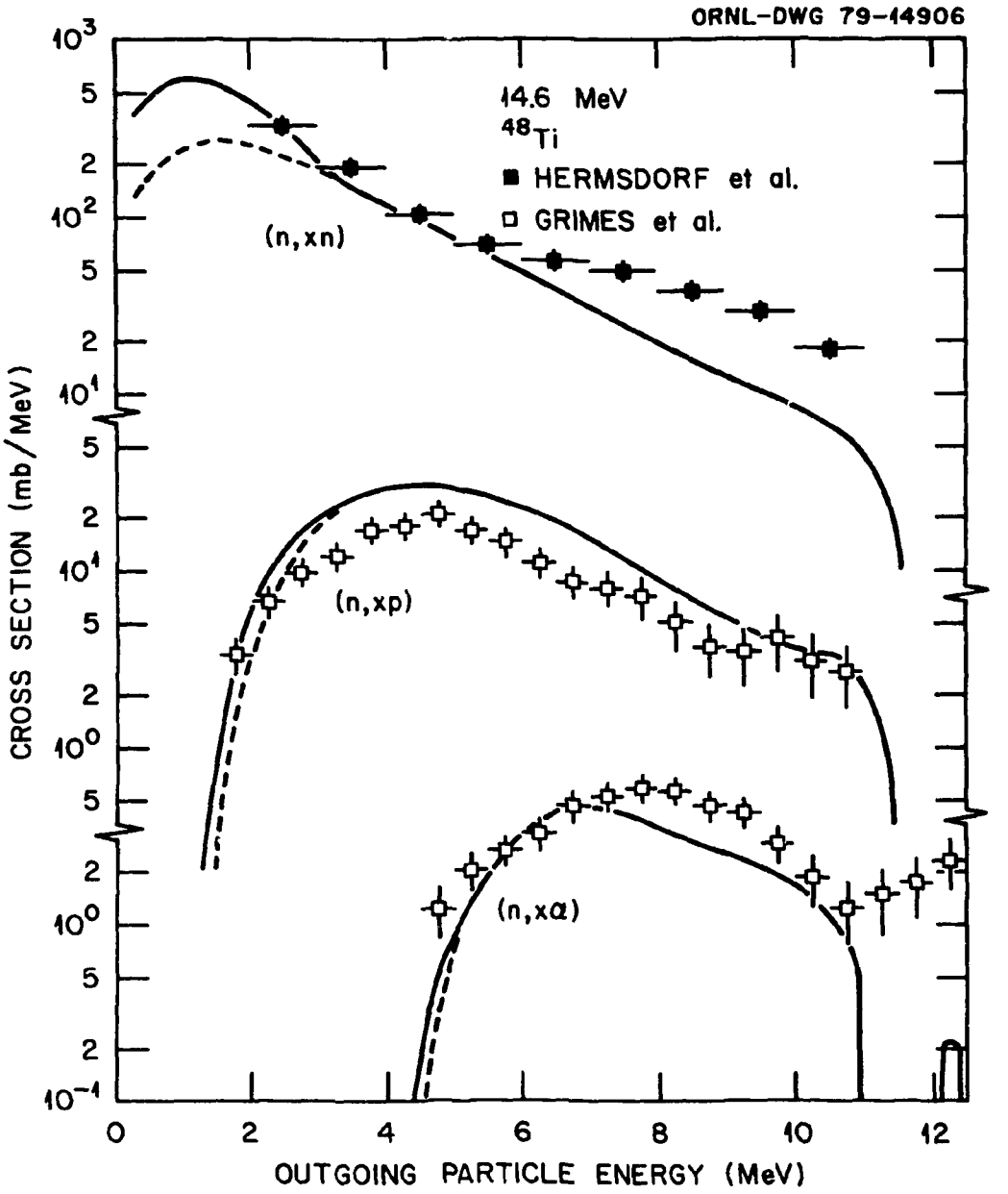

Fig. 8. Calculated and experimental n, p, α production spectra from 14.6-MeV neutrons on ^{48}Ti.

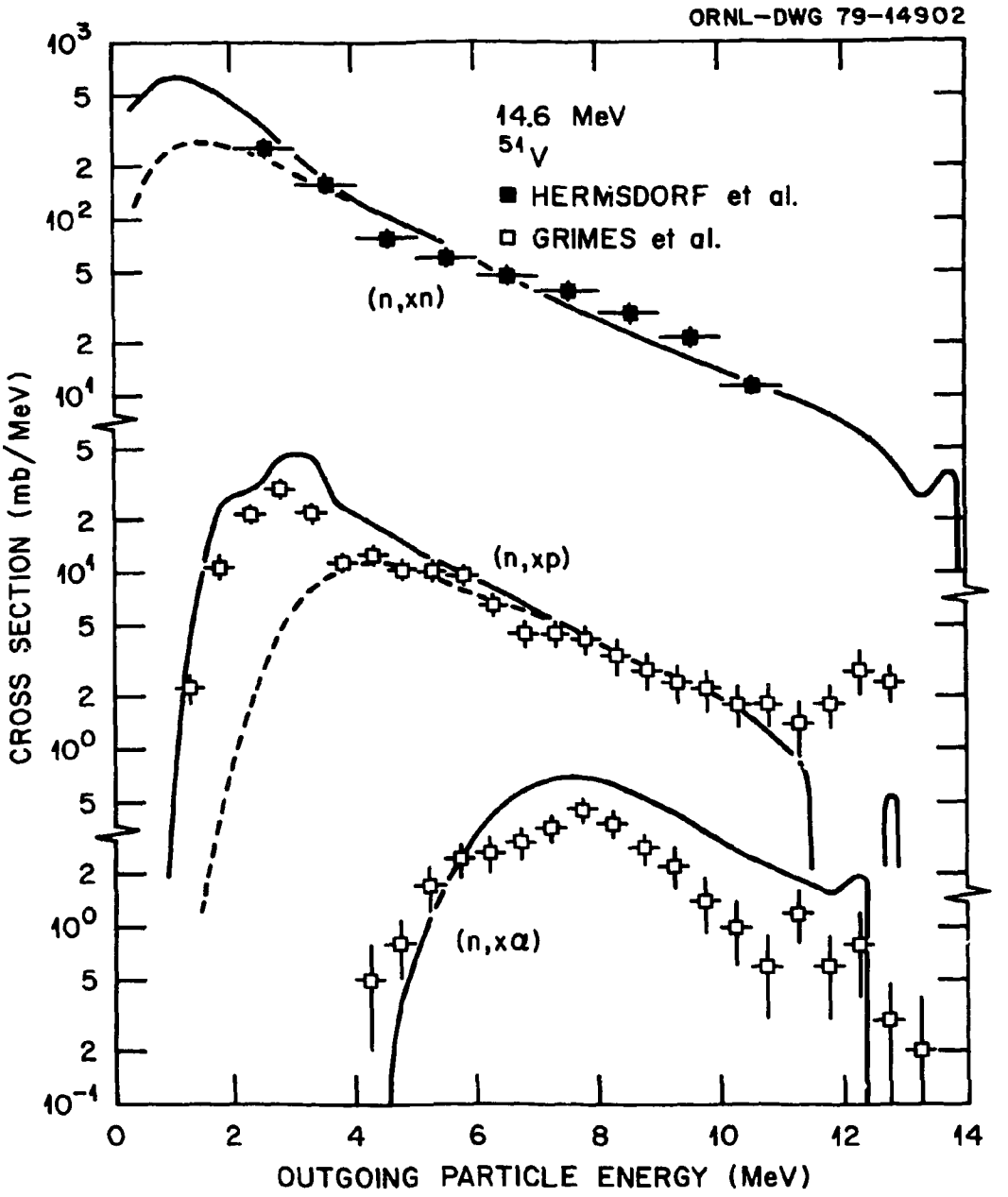

Fig. 9. Calculated and experimental n, p, α production spectra from 14.6-MeV neutrons on ^{51}V.

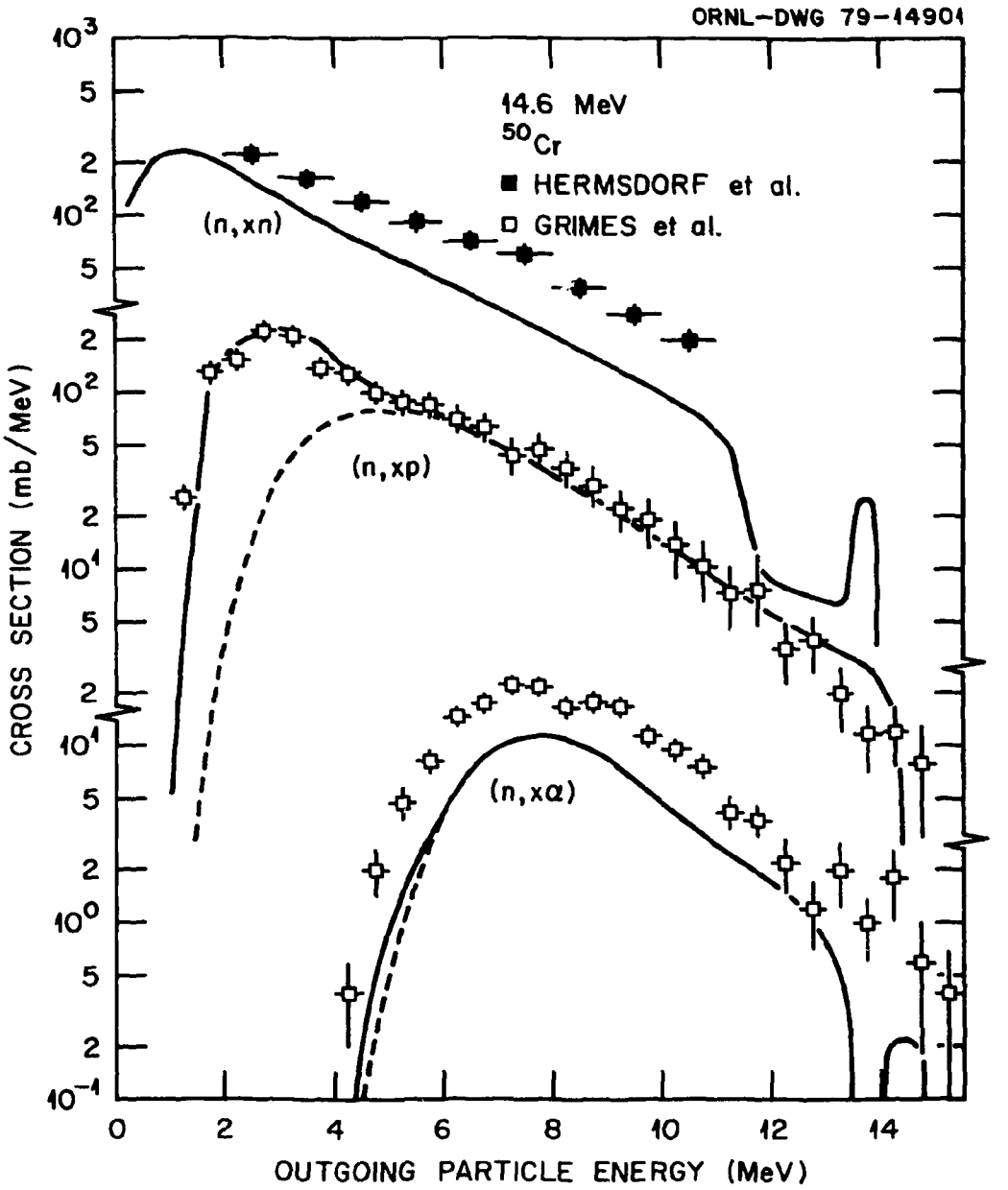

Fig. 10. Calculated and experimental n, p, α production spectra from 14.6-MeV neutrons on ^{50}Cr.

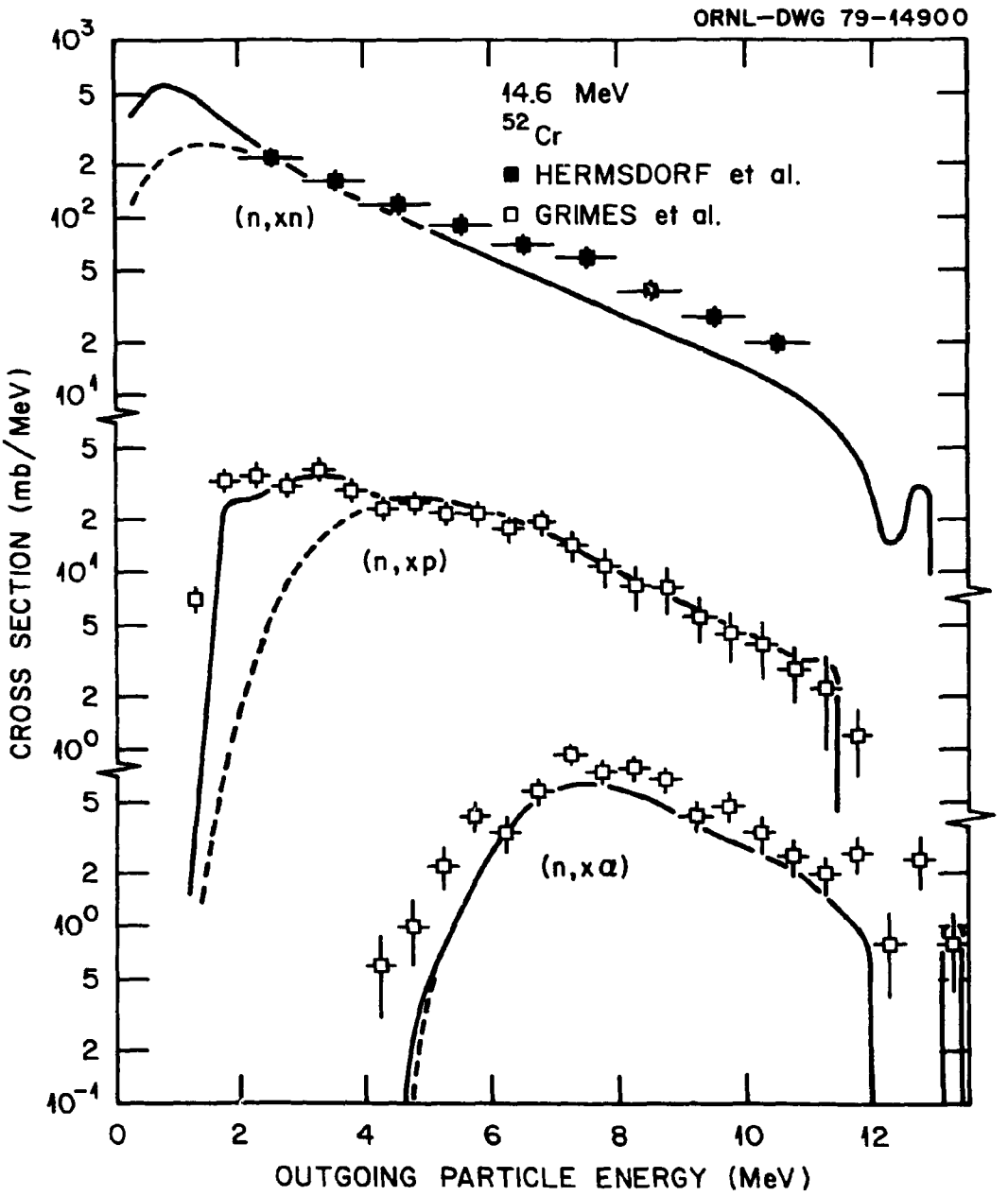

Fig. 11. Calculated and experimental n, p, α production spectra from 14.6-MeV neutrons on ^{52}Cr.

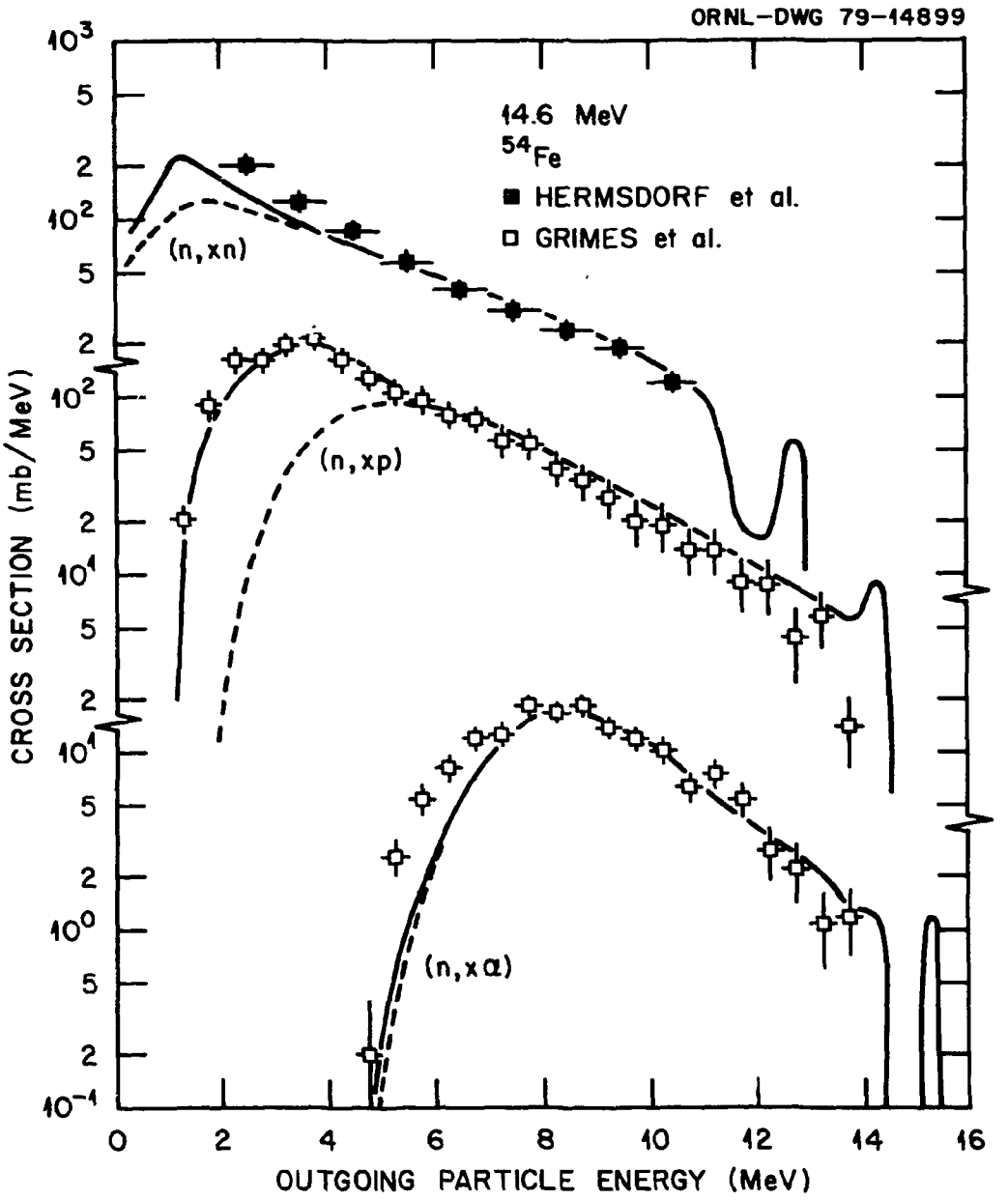

Fig. 12. Calculated and experimental n, p, α production spectra from 14.6-MeV neutrons on ^{54}Fe.

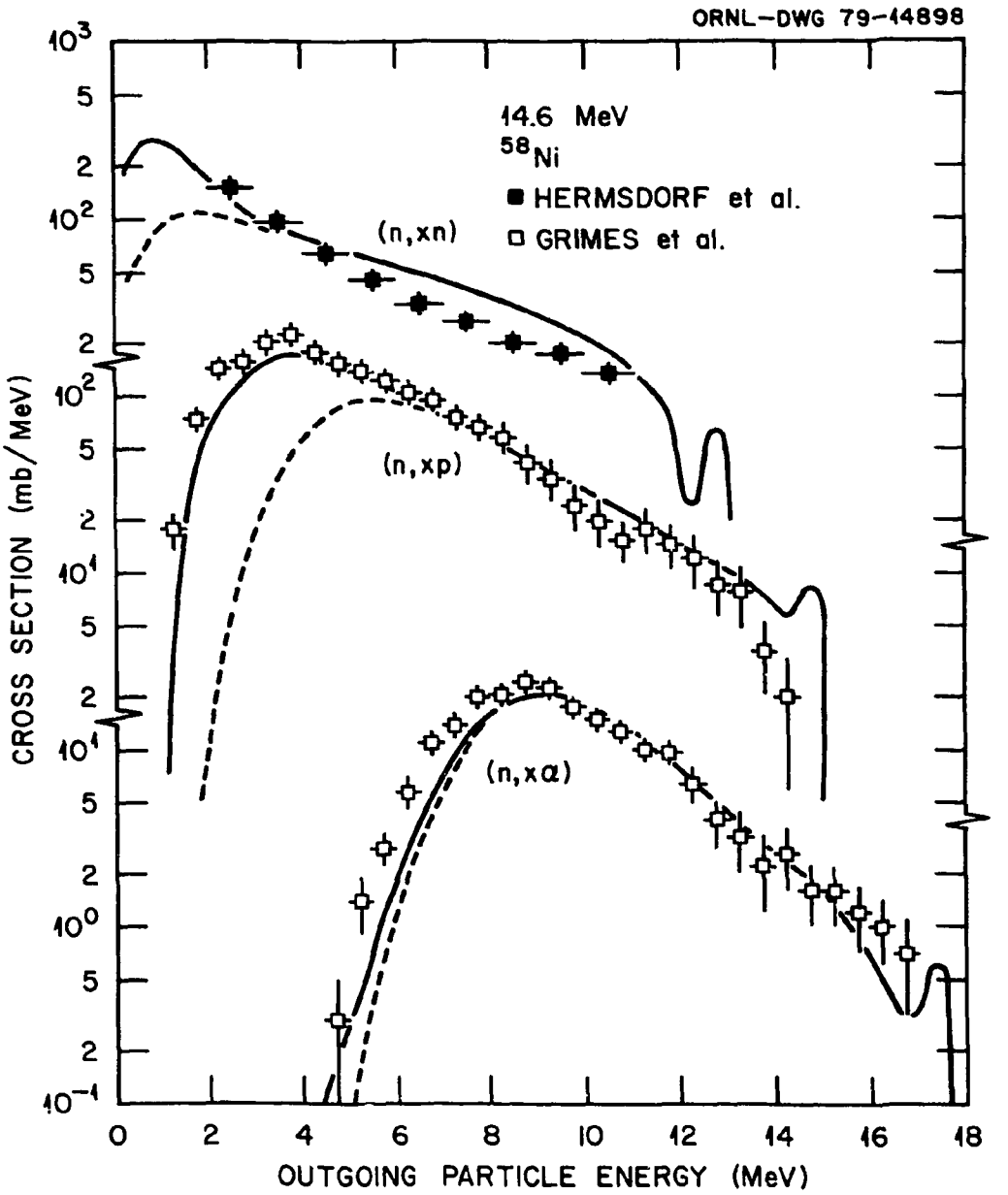

Fig. 13. Calculated and experimental n, p, α production spectra from 14.6-MeV neutrons on ^{58}Ni.

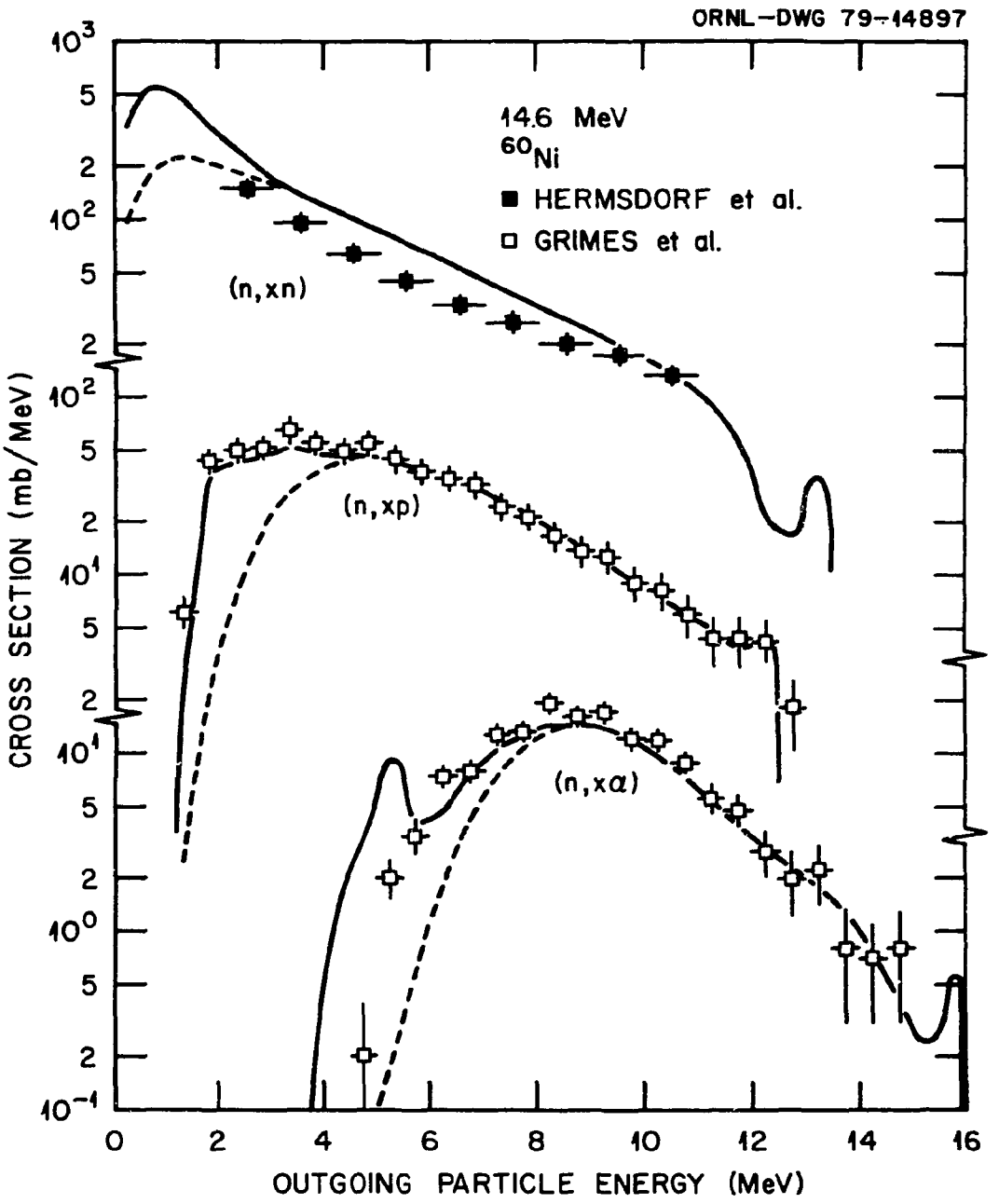

Fig. 14. Calculated and experimental n, p, α production spectra from 14.6-MeV neutrons on ^{60}Ni.

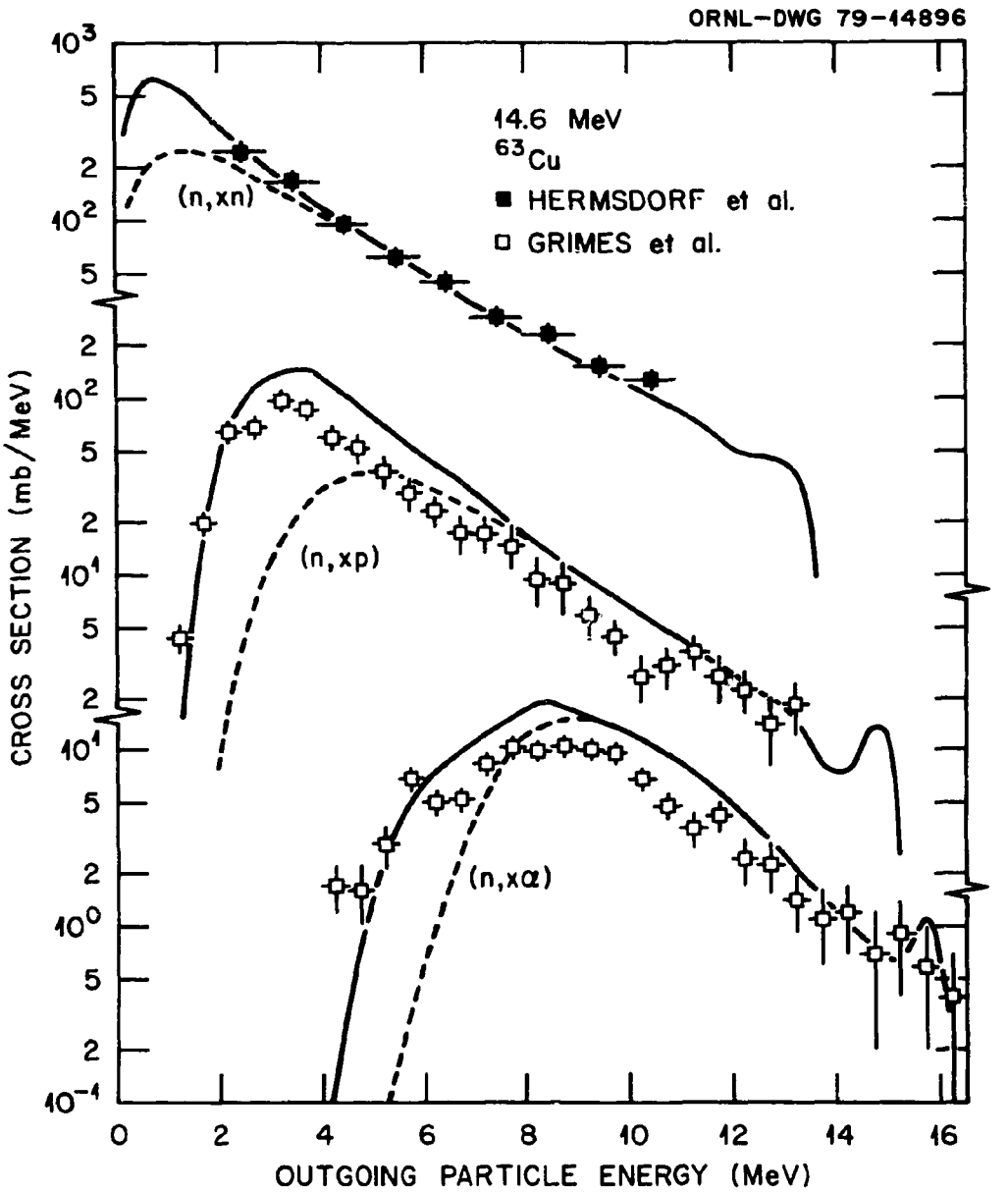

Fig. 15. Calculated and experimental n, p, α production spectra from 14.6-MeV neutrons on ^{63}Cu.

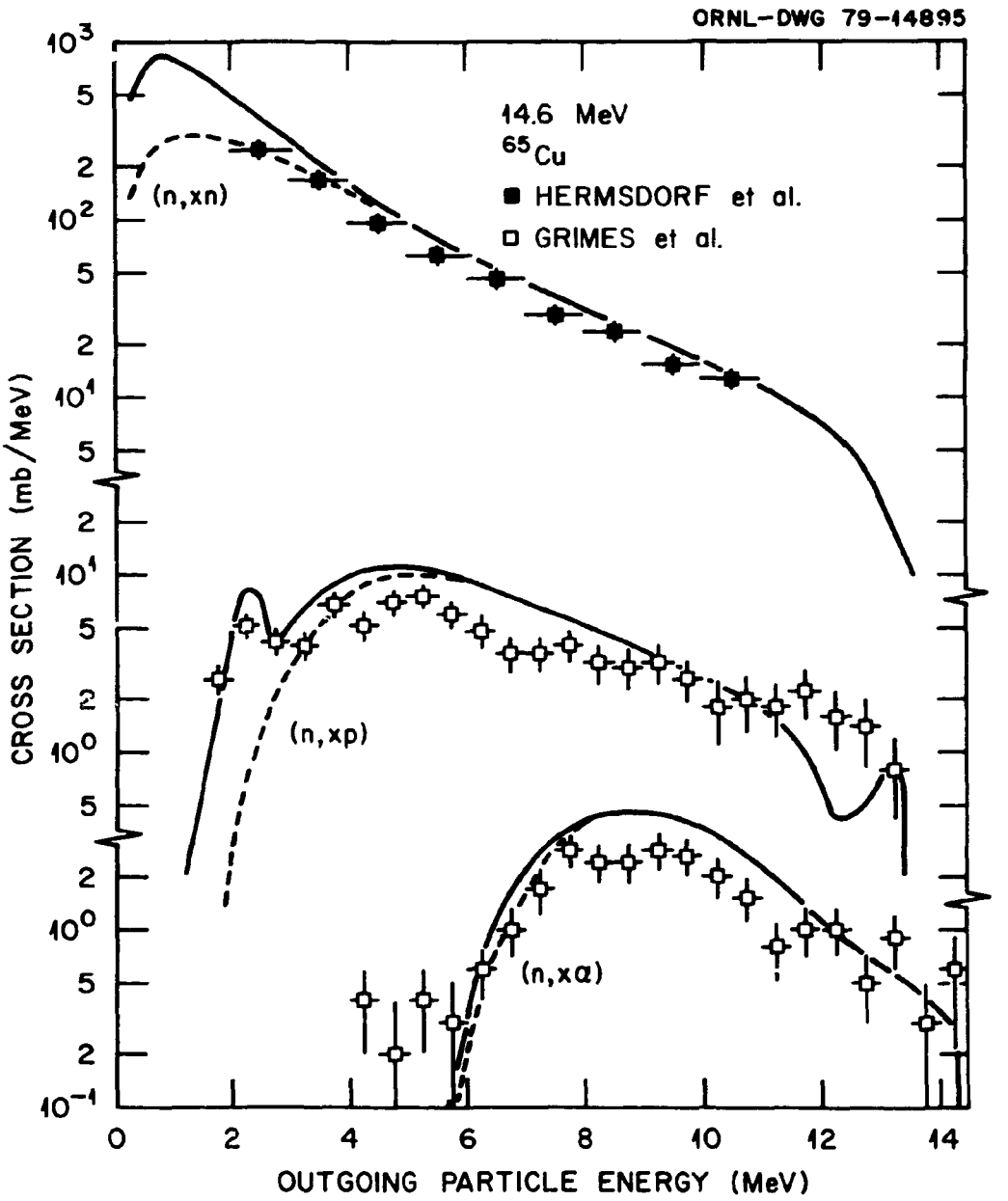

Fig. 16. Calculated and experimental n, p, α production spectra from 14.6-MeV neutrons on ^{65}Cu.

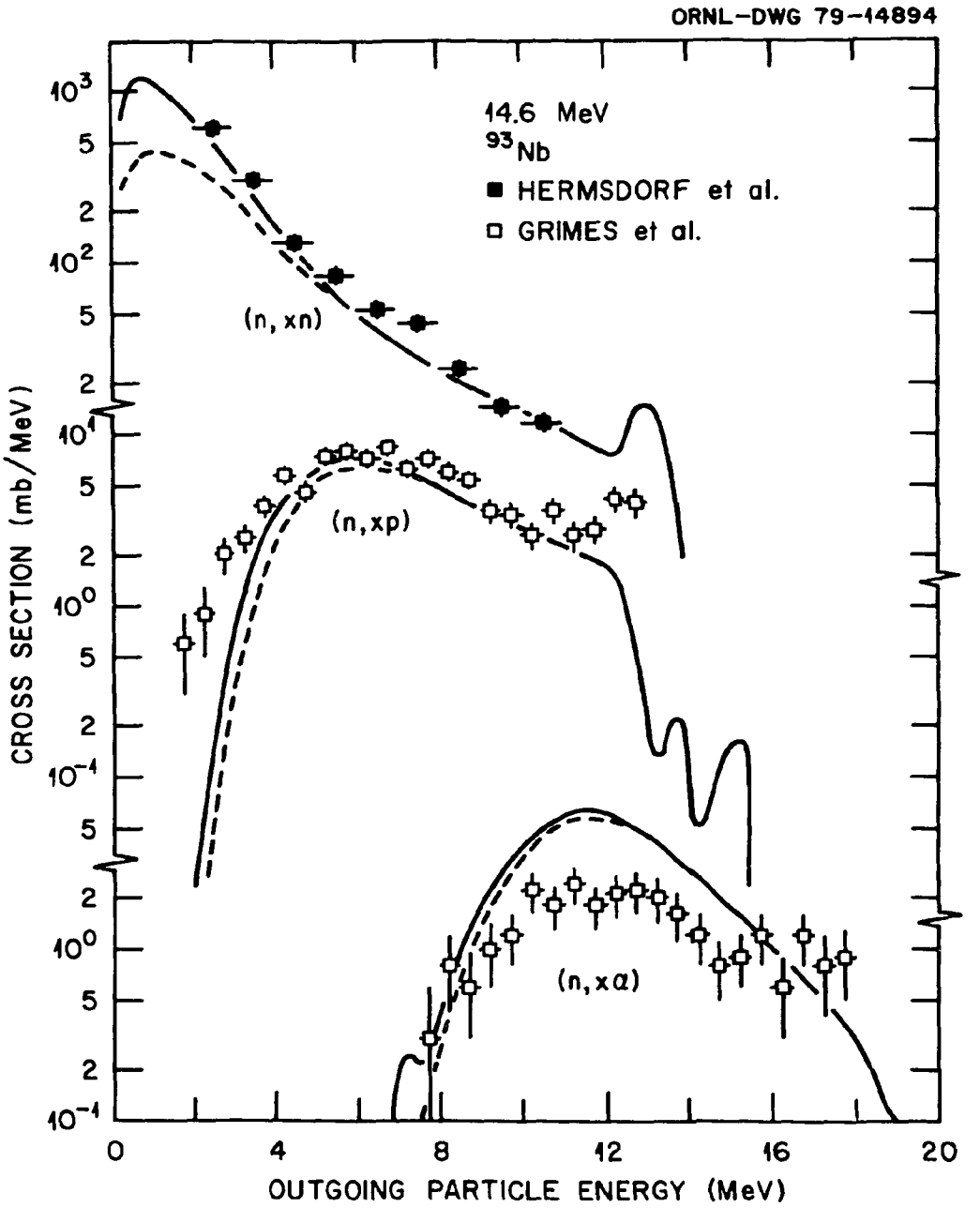

Fig. 17. Calculated and experimental n, p, α production spectra from 14.6-MeV neutrons on ^{93}Nb.

ORNL/TM-7042

INTERNAL DISTRIBUTION

1-5. L. S. Abbott
6. R. G. Alsmiller, Jr.
7. G. de Saussure
8-12. C. Y. Fu
13. H. Goldstein (Consultant)
14. J. A. Harvey
15. D. J. Horen
16. C. H. Johnson
17. D. C. Larson
18-22. F. C. Maienschein
23. B. F. Maskewitz
24-28. R. W. Peelle
29. F. G. Perey
30. D. Steiner
31. P. H. Stelson
32. A. Zucker
33. Paul Greebler (Consultant)
34. W. B. Loewenstein (Consultant)
35. Richard Wilson (Consultant)
36-37. Central Research Library
38. ORNL Y-12 Technical Library
39. Laboratory Records Department
40. ORNL Patent Office
41. Laboratory Records (RC)

EXTERNAL DISTRIBUTION

42. E. D. Arthur, Los Alamos Scientific Laboratory, Los Alamos, NM 87545
43. S. M. Austin, Cyclotron Laboratory, Michigan State University, East Lansing, MI 48824
44. David Auton, Defense Nuclear Agency, Tactical Nuclear Division, Washington, DC 20305
45. M. Blann, University of Rochester, Rochester, NY 14627
46. Robert C. Block, Nuclear Engineering & Science Department, Rensselaer Polytechnic Institute, Troy, NY 12181
47. Charles D. Bowman, Radiation Division, National Bureau of Standards, Washington, DC 20234
48. Robert E. Chrien, Brookhaven National Laboratory, Upton, NY 11973
49. M. Divadeenam, Brookhaven National Laboratory, Upton, NY 11973
50. Donald Gardner, L-405, Lawrence Livermore Laboratory, P.O. Box 808, Livermore, CA 94550
51. Philip B. Hemmig, Reactor Physics Branch, Div. of Reactor Research and Technology, DOE, Washington, DC 20545
52. R. J. Howerton, L-71, Lawrence Livermore Laboratory, P.O. Box 808, Livermore, CA 94550
53. C. Kalbach-Walker, Duke University, Durham, NC 27706
54. B. R. Leonard, Battelle-Northwest, P.O. Box 999, Richland, WA 99352
55. D. Madland, Los Alamos Scientific Laboratory, Los Alamos, NM 87545
56. F. M. Mann, W/Fed. 429, Westinghouse Hanford, P.O. Box 1970, Richland, WA 99352
57. P. Moldauer, Argonne National Laboratory, Argonne, IL 60439
58. A. Prince, Bldg. 197D, National Nuclear Data Center, Brookhaven National Laboratory, Upton, NY 11973

59. Robert Schenter, Hanford Engineering Development Laboratory, P.O. Box 1970, Richland, WA 99352
60. A. B. Smith, Bldg. 314, Reactor Eng. Div., Argonne National Laboratory, 9700 South Cass Ave., Argonne, IL 60439
61. Stanley Whetstone, Division of Basic Energy Sciences, DOE, Washington, DC 20545
62. P. G. Young, Los Alamos Scientific Laboratory, Los Alamos, NM 87545
63. Assistant Manager, Energy Research and Development, DOE-ORO, Oak Ridge, TN 37830

64-90. Technical Information Center, Oak Ridge